On the nature of wind-forced upwelling in Barrow Canyon

Maria N. Pisareva[a, *], Robert S. Pickart[b], Peigen Lin[b], Paula S. Fratantoni[c], Thomas J. Weingartner[d]

[a]*P.P. Shirshov Institute of Oceanology RAS; 36, Nakhimovski prospect, Moscow, 117997, Russia*

[b]*Woods Hole Oceanographic Institution; 266 Woods Hole Rd., Woods Hole, MA, 02543, USA*

[c]*Northeast Fisheries Science Center; 166 Water Street, Woods Hole, MA, 02543, USA*

[d]*University of Alaska Fairbanks; 505 South Chandalar Drive, Fairbanks, AK, 99775, USA*

*Corresponding author. Tel. +79166667555
E-mail address: mnpisareva@gmail.com (M. N. Pisareva)

ABSTRACT

Using time series from a mooring deployed from 2002–2004 near the head of Barrow Canyon, together with atmospheric and sea-ice data, we investigate the seasonal signals in the canyon as well as aspects of upwelling and the wind-forcing that drives it. On average, the flow was down-canyon during each month of the year except February, when the up-canyon winds were strongest. Most of the deep flow through the head of the canyon consisted of cold and dense Pacific-origin winter water, although Pacific-origin summer waters were present in early autumn. Over the two-year study period there were 54 upwelling events: 33 advected denser water to the head of the canyon, while 21 upwelled lighter water due to the homogeneous temperature/salinity conditions during the cold season. The upwelling occurs when the Beaufort High is strong and the Aleutian Low is deep, consistent with findings from previous studies. Most events resulted in the reintroduction of Pacific Winter Water onto the Chukchi Shelf, rather than advection of Atlantic Water. Overall there were more than twice as many upwelling events during the cold season as the warm season due to the seasonal strengthening of the winds. An analysis of temporally integrated measures revealed a statistically significant relationship between the atmospheric forcing and upwelling response, such that stronger storms tend to result in stronger upwelling. Finally, it is demonstrated that upwelling typically corresponds to the occurrence of the Northeast Chukchi Polynya.

Keywords: Arctic Ocean, Barrow Canyon, Upwelling, Polynya, Pacific-origin water masses, Atlantic Water

1. Introduction

The Pacific-origin water that flows northward through Bering Strait has a profound impact on the physical state of the western Arctic Ocean as well as the ecosystem. It carries large amounts of freshwater and heat (e.g. Steele et al., 2004; Shimada et al., 2006; Woodgate et al., 2012) and is also a significant source of nutrients, phytoplankton and zooplankton to the region (e.g. Codispoti et al., 2005; Lowry et al., 2015; Ershova et al., 2015). Upon entering the wide and shallow Chukchi Sea, the water is channeled by the bottom topography of the shelf and is also influenced and/or transformed by strong atmospheric forcing and the seasonal presence of sea ice. There are three main pathways that the Pacific water follows on its way northwards (Fig. 1): the western branch, which advects the water into Herald Canyon; the middle branch that proceeds through the Central Channel between Herald and Hanna Shoals; and the eastern branch, which flows adjacent to the west coast of Alaska. Some of the water in the western and central branches is diverted to the east and ultimately enters Barrow Canyon (Weingartner et al., 2005; Pickart et al., 2010; Pickart et al., 2016; see Fig. 1).

The Pacific Water exits the Chukchi Shelf through Long Strait, Herald Canyon, and Barrow Canyon. Averaged over the course of the year the division in transport between the three exit points is believed to be comparable (Woodgate et al., 2005a). Some of the water leaving Herald Canyon forms an eastward-flowing shelfbreak jet along the edge of the Chukchi Sea (Corlett and Pickart, 2017; Li et al., 2019), while some of the water exiting Barrow Canyon forms an eastward-flowing shelfbreak jet along the edge of the Beaufort Sea (Nikolopoulos et al., 2009; Brugler et al., 2014). Using historical shipboard hydrographic and velocity data, Corlett and Pickart (2017) recently demonstrated that a significant amount of the northward transport from Barrow Canyon is diverted to the west and forms a current along the continental slope of the Chukchi Sea (offshore of the shelfbreak jet). This has been named the Chukchi Slope Current, and, based on mooring data, it is present year-round (Li et al., 2019). In addition to these localized advective outflows, water from the Chukchi Shelf is believed to be fluxed seaward all along the shelfbreak via turbulent processes (Pickart et al., 2005; Spall et al., 2008) and via subduction (Timmermans et al., 2014).

It has been argued that, during the summer months, a significant fraction of the transport of Pacific Water flowing through Bering Strait is channeled into Barrow Canyon. Using a long-term transport proxy constructed from mooring and wind data, Weingartner et al. (2017) estimated that ~40 % of the Bering Strait inflow drains into the canyon during the months of May–September. Based on shipboard measurements, it appears that, at times, this percentage can be as large as 80–

100% (Itoh et al., 2013; Gong and Pickart, 2016; Pickart et al., 2016). The year-long mean transport at the head of the canyon is estimated to be ~0.2 Sv (Weingartner et al., 2017), while at the mouth of the canyon it is estimated to be ~0.45 Sv (Itoh et al., 2013). This makes the canyon a particularly important gateway for Pacific Water entering the basin. In addition to the two currents that emanate from Barrow canyon, eddies and other turbulent features are spawned there that propagate into the basin (e.g. Pickart and Stossmeister, 2008).

Barrow Canyon is also known to be a biological "hotspot" due to its elevated nutrient concentrations, enhanced productivity rates, and high benthic biomass. Consequently, it is a region where marine mammals and seabirds concentrate (Hill and Cota, 2005; Grebmeier et al., 2015). As such, Barrow Canyon was included as one of the original sites of the Distributed Biological Observatory (DBO) program when the program was initiated in 2010. As described by Moore and Grebmeier (2018), the aim of DBO is to enhance our understanding of the Pacific Arctic ecosystem and document the ongoing changes within it, focusing on key hotspot regions and how they are changing in time. Part of the goal of DBO is to better interpret the biological responses in light of the physical variability. Therefore, investigation of the physical processes occurring in Barrow Canyon is highly relevant for the DBO program.

Several mechanisms bring nutrient-rich Pacific Winter Water into the canyon that likely influence the productivity there. The flow pathways noted above seasonally advect this cold water into the head of the canyon. The coastal branch is the dominant source during the winter months into late-spring (Pickart et al., 2016; Weingartner et al., 2017), while the central pathway transports the cold water into the canyon during mid- to late-summer (Pickart et al., this issue). In addition to these advective sources, enhanced small-scale mixing in the canyon (Shroyer, 2012) likely fluxes nutrients from the sediments into the water column. Bottom boundary layer detachment has been identified in Herald Canyon as another means of fluxing nutrients vertically from the seafloor (Pickart et al., 2010), and it is likely that this mechanism also operates in Barrow Canyon. Shipboard measurements support this notion (R. Pickart, unpublished data).

A particularly energetic process that occurs in Barrow Canyon is that of upwelling, which can bring nutrient-rich winter water from offshore into the canyon and onto the Chukchi Shelf. The importance of this cold water for the regional ecosystem cannot be overstated. It is known to trigger phytoplankton blooms in the region (and even maintain under-ice blooms), which have been observed to be sustained for long periods of time in the presence of this water mass (Lowry et al., 2015). Enhanced primary production, in turn, leads to the increases in biological production across all trophic levels. Warm Atlantic Water, which resides below the winter water in the interior basin

(and is also rich in nutrients), can also be upwelled onto the Chukchi Shelf. At times, it is advected far south of the canyon (Bourke and Paquette, 1976) and can influence the formation and maintenance of the Northeast Chukchi Polynya (Ladd et al., 2016; Hirano et al., 2016). In addition, upwelling plays a role in other processes on the shelf, such as water mass transformation (i.e. Kawaguchi et al., 2011), ice freeze-up and melt, and eddy formation. It can also affect the properties of the waters that ultimately enter the Arctic basin (i.e. Weingartner et al., 2017).

Numerous factors are believed to drive the up-canyon flow in Barrow Canyon. These include propagation of shelf-edge waves (Aagaard and Roach, 1990; Carmack and Kulikov, 1998; Danielson et al., 2014), changes in the meridional sea level pressure gradient (Mountain et al., 1976), and southward rectified flow at depth due to temporal variations in the outflow of the Pacific water (Signorini et al., 1997). However, the most common upwelling mechanism in Barrow Canyon is wind forcing, in particular enhanced easterly and northeasterly winds (e.g. Carmack and Kulikov, 1998; Pickart et al., 2009; Watanabe, 2011; Okkonen et al., 2009). Despite the previous work addressing upwelling in Barrow Canyon, there are numerous aspects of this process that warrant further study. This includes the precise relationship between the currents and the water masses in the canyon. There is also the need for an improved understanding of how the hydrography and flow are affected by the wind and the associated large-scale atmospheric circulation patterns, as well as by the presence of sea ice and occurrence of polynyas.

In this study, we use two years of mooring data collected near the head of Barrow Canyon, together with atmospheric reanalysis fields, meteorological data, and satellite ice concentration data, to investigate different aspects of wind-driven upwelling in Barrow Canyon. The data are first used to characterize the flow and atmospheric forcing in the canyon, as well as the seasonality of the water masses. This allows us to then more effectively describe the anomalous conditions associated with upwelling. We also investigate the differences between the two years, which emphasizes the pronounced interannual variability that occurs in the canyon. The mooring was situated in close proximity to two of the DBO lines: DBO-4, which is a transect to the northwest of Wainwright, Alaska, and DBO-5, which crosses the central portion of Barrow Canyon (see Moore and Grebmeier (2018) for the locations of all eight DBO lines). Although the mooring data were not collected contemporaneously with the DBO program, the physical processes analyzed here will greatly aid in the interpretation of the ongoing DBO measurements.

2. Data and Methods

The primary in-situ data used in this study come from the Western Arctic Shelf-Basin Interactions (SBI) program, which took place from 2002–2004 (Grebmeier et al., 2005). While more recently collected mooring data from the vicinity of Barrow Canyon have been used to address certain aspects of upwelling (e.g. Ladd et al., 2016; Weingartner et al., 2017), the results presented here offer new insights into this process, and also allow for a future comparison of conditions between the early 2000s and roughly a decade later. We now describe the different sources of data used in our study.

2.1. Mooring data

A mooring was maintained near the head of Barrow Canyon at the 78-m isobath (Fig. 2) as part of the SBI program from August 2002 to September 2004. The canyon is O(50 km) wide and O(150 km) long, extending from approximately the 50-m isobath to the 300-m isobath. The mooring was equipped with a Sea-Bird Electronics SBE16 SEACAT, which provided time series of temperature, salinity, and pressure every hour at 67 m depth. The SEACAT was calibrated at Sea-Bird before and after each deployment. Hourly velocity data (flow speed and direction) were obtained from an AANDERAA Recording Current Meter (ACM-7) at 64 m depth. These data were detided by estimating the tidal signal using the T_Tide harmonic analysis toolbox (Pawlowicz et al., 2002) and then removing it from the velocity time series. As the current fluctuations at the head of the canyon are maximized along the canyon axis, we rotated our velocity data into a coordinate frame with a positive alongstream direction of 56ºT (down-canyon) and positive cross-stream direction of 326ºT (toward the Chukchi Shelf). This choice was guided by the orientation of the principal axis of the variance ellipse and by the orientation of the mean flow (Fig. 2). Weingartner et al. (2017) used a similar rotation angle. The SEACAT returned a complete data set for both deployments (with a gap of a few days during the mooring turnaround). However, the AANDERAA current meter failed in summer 2003, so there is a three-month gap in the velocity time series at the end of the first year.

2.2. Barrow wind data

Data from the meteorological station at Barrow, Alaska (now called Utqiagvik, Alaska) are used to characterize the wind forcing in the region. The station is located approximately 110 km to the northeast of the mooring site (Fig. 2). Hourly data were obtained from the National Climate Data Center of the National Oceanic and Atmospheric Administration (NOAA). As described in

Pickart et al. (2013), the data were subsequently quality controlled and interpolated to fill in small gaps. We determined the component of the wind that resulted in the maximum correlation with the along-canyon current fluctuations at the head of the canyon. In the analysis that follows, positive winds (southwesterly) are directed along 52°T, and negative winds (northeasterly) are directed along 232°T.

2.3. Atmospheric reanalysis fields

To characterize the large-scale atmospheric patterns, we use the North American Regional Reanalysis (NARR, Mesinger, 2006) sea level pressure (SLP) data and 10 m winds. NARR uses newer data assimilation techniques and more advanced modeling procedures than the original National Centers for Environmental Prediction (NCEP) global reanalysis product. The spatial resolution of the NARR data is 32 km, and the time increment is 6 hours.

2.4. Satellite ice concentration data

For sea-ice concentration, we use the blended Advanced Very High Resolution Radiometer (AVHRR) and the Advanced Microwave Scanning Radiometer (AMSR) product of National Climatic Data Center, NOAA. This combined product, with two different types of sensors, helps reduce systematic errors and avoids data gaps in cloudy regions (Reynolds et al., 2007). The combined product is available from 2002 through September 2011; for the period of 2011 – 2017 AVHRR time series were used. The spatial resolution of the data is 0.25°, and the temporal resolution is once per day. The estimated accuracy of the ice concentration data is ±10% (Cavalieri et al., 1991).

3. Hydrographic and flow characteristics at the head of Barrow Canyon

Before investigating the upwelling in Barrow Canyon, it is necessary to describe the different types of water found in the canyon, their seasonality, and the overall character of the flow. The two-year mean velocity vector (~20 cm s^{-1} down-canyon) is shown in Fig. 2, along with the mean 10-m wind vector at Barrow (~2 m s^{-1} directed roughly up-canyon). Previously reported flow measurements in the canyon have also shown a mean northward velocity of 15–20 cm s^{-1} that opposes the wind (Mountain et al., 1976; Weingartner et al., 2017), with velocities frequently exceeding 50 cm s-1 (see also Weingartner et al. (2005) and Gong and Pickart (2005)).

3.1. Water masses

In this study, we use potential temperature-salinity (T/S) ranges for the different water masses following previous studies (e.g. Coachman et al., 1975; Gong and Pickart, 2015; Itoh et al., 2015). These definitions are shown in Fig. 3. We note that these limits are not precise since the T/S characteristics of the water masses entering the Chukchi Sea can vary from year to year, but for our purposes this classification is sufficient.

As depicted in Fig. 1, Pacific Water enters Barrow Canyon both from the coastal branch and from the Central Channel branch. Over the course of the year, these two pathways deliver all of the different types of Pacific-origin water to the canyon (Fig. 3). The two classes of summer water include Alaskan Coastal Water (ACW) and Bering Summer Water (BSW). The former originates from river run-off into the Gulf of Alaska and eastern Bering Sea and enters the Chukchi Sea in the Alaskan Coastal Current (ACC). The latter is a combination of nutrient-rich Gulf of Anadyr water and colder and fresher Bering Shelf waters that mix north of Bering Strait (Coachman et al., 1975). BSW is advected into Barrow Canyon via both the central and coastal pathways (Gong and Pickart, 2005).

Previous studies (e.g. Brugler et al., 2014; Pickart et al., 2016) have considered two types of Pacific-origin winter water: newly-ventilated winter water (i.e. water that was recently modified by convective overturning either on the northern Bering Shelf or Chukchi Shelf), and remnant winter water (RWW, which is older winter water that has been warmed by solar heating and/or via mixing with summer waters). Here we also distinguish between two classes of newly-ventilated winter water following Weingartner et al. (1998; 2017) and Itoh et al. (2015) (and others) who demonstrated that the water can be further salinized within polynyas on the Chukchi Shelf. The

polynya product is termed hypersaline winter water (HSWW), while the more moderately salinized product is referred to here simply as winter water (WW).

The remaining two water masses found in Barrow Canyon are Atlantic Water (AW) and fresh surface water of local Arctic origin influenced by ice melt and/or river discharge (referred to here as meltwater (MW) following Pisareva et al., 2015 and others). As discussed in the introduction, AW is often advected into the canyon during upwelling events. This water originates from the Eurasian Arctic and typically resides deeper than about 200 m in the Canada Basin. It is transported throughout the Arctic Ocean by a system of cyclonic boundary currents (e.g. Rudels et al., 2004). MW is typically observed in the upper part of the water column and is found over a large range of temperatures depending on the time of year. River water is distinguishable from meltwater using specialized tracers (e.g. the stable oxygen isotope O-18; see Cooper et al., 1997), but our data do not allow us to make this distinction; note also that our hydrographic sensor was situated near the bottom.

3.2. Seasonality

On average, the flow at the head of Barrow Canyon during the 2-year measurement period was down-canyon during each month of the year except February (Fig. 4a). The maximum flow occurred in summer, with a peak in July of nearly 50 cm s^{-1}. The error bars shown in Fig. 4 are standard errors, hence it is seen that the down-canyon flow during part of the fall (October-November) was not significantly different from zero. The seasonal cycle of wind (Fig. 4b) reveals that the up-canyon flow in February corresponded to the month with the strongest up-canyon winds. The measurements at the head of the canyon reported by Weingartner et al. (2017) for the period 2010–15 also show the strongest down-canyon flow in summer. However, from December through April the flow was up-canyon or near zero for their dataset, hence during our earlier measurement period the currents were more consistently directed out of the canyon. This might be related to the more persistent easterly/northeasterly winds in the later period versus our measurement period (e.g. Brugler et al., 2014). The potential temperature and salinity at the head of the canyon also displayed seasonality (Fig. 4c). From January to May the water was near the freezing point, then warmed to a maximum temperature in September before progressively getting colder through the remainder of the fall. The salinity was lowest in the summer and early-fall.

To identify the water masses flowing through the canyon over the two-year period we constructed a T/S diagram for each season, which includes a histogram of the measurements (Fig. 3). During the summer months (June–August), most of the deep water at the canyon head

consisted of WW and RWW. As explained in Pickart et al. (this issue), these two winter waters are still flushing down the canyon in summer due to the long advective route of the central pathway (see also Weingartner et al., 2005; Pickart et al., 2016; Shroyer and Pickart, 2017). The next most common water mass was BSW, with only a small amount of ACW. During the fall (September–November), both summer water masses were present (mainly in the early-fall) but again there was a large presence of RWW. Substantial quantities of AW were measured as well, due to upwelling activity. MW was also observed in this deep part of the water column. The winter (December–February) and spring (March–May) seasons were characterized by the largest volumes of dense winter water, including HSWW near the freezing point. Interestingly, there were two modes of the winter water: a WW mode near a salinity of 32.5, and a HSWW mode in the salinity range of 34–34.5. While AW was present during the winter (along with small amounts of RWW and BSW), the spring months were characterized almost exclusively by newly ventilated winter water near the freezing point.

Using the definitions of the water masses, we created a time series that reveals when each was present at the head of the canyon (Figure 5). Consistent with the seasonal T/S plots, the dominant water mass was the cold winter water (both WW and HSWW), which was present for prolonged periods during the two year-long deployments. There was considerably more HSWW the first year. RWW appeared in June of each year, interspersed with the WW (this is when the winter water starts to warm). The two summer waters tended to appear in patches, sometimes lasting only a few days. Consistent with the findings of von Appen and Pickart (2012), the BSW appeared earlier in the summer than the ACW, and lasted later into the fall (as late as mid-December the second year). There was far less ACW in the second summer, only a very small amount in August and then again in September. The AW, which appeared only in fall and winter, sometimes persisted for close to a week, while other times only for a day or so. Finally, while MW is commonly observed in Barrow Canyon in summer, it typically resides in the upper 20–30 m (Itoh et al., 2015; Pickart et al., this issue). We measured water with the characteristics of MW at 67 m in late-November/early-December of the second year. Some of this was near the freezing point (Fig. 3c), suggesting melting of ice that had only recently been formed. As for the warmer MW, it is possible that this resulted from mixing of RWW with very fresh surface waters, or ACW that had been cooled in the fall.

Based on our mooring data from 2002–2004, almost 80% of the deep flow through the head of the canyon consisted of cold and dense winter waters: WW (38%), RWW (31%) and HSWW (10%). This is in line with previous studies (e.g. Weingartner et al., 2017). However, one should remember that these estimates only apply to the near-bottom layer and hence are not representative

295 of the total flow discharge through the head of the canyon. BSW was present at the mooring site
296 12% of time, while ACW was only measured 3% of time. Note that this does not imply that the
297 ACC was this sporadic. The ACW advected by the current is often confined to shallower depths in
298 the canyon (see Pickart et al., this issue). In total, AW was observed 4% of the time, which was
299 associated with upwelling (either up-canyon flow during the event or return flow back to the basin
300 after the event). MW was measured less than 2% of time.
301

4. Atmospheric forcing and sea ice

We now assess the atmospheric conditions both during the study period and climatologically for the region, as well as the sea ice cover.

4.1. Sea level pressure and winds

It is well known that two atmospheric centers of action – the Beaufort High (BH) and the Aleutian Low (AL) – govern the wind patterns across the Chukchi Shelf (Pickart et al., 2009, 2013; Brugler et al., 2014). Using the Barrow weather station wind data, we computed the monthly mean along-canyon winds averaged over the period 1979 – 2014. One sees that, climatologically, the winds are out of the northeast during each month of the year (cyan curve in Fig. 4b). There is a well-defined seasonal cycle, with stronger winds during fall and winter, although the amplitude is only about 1 m s^{-1}. The large standard errors indicate significant interannual variability within each month.

To put this in context we constructed climatological maps of SLP and 10-m winds using the 35-year NARR reanalysis dataset (Figure 6). Following Woodgate et al. (2005a), we defined the cold season from October to March and the warm season from April to September. During the warm period, the BH is climatologically centered over the Beaufort Sea, with a weak signature of the AL situated in the eastern Bering Sea. In winter, the BH strengthens, spreads to southwest, and merges with the Siberian High – a system of high pressure over Siberia associated with anti-cyclonic circulation. At the same time the AL deepens significantly due to the greater number and increased strength of storms progressing along the North Pacific storm track (e.g. Favorite et al., 1976; Pickart et al., 2009; Lin et al., 2016). As such, the SLP gradient between the two centers of action is enhanced in the cold season, which leads to stronger winds in the Chukchi Sea.

Not surprisingly, there are differences between the studied period versus the climatological winds (compare Figs. 6 and 7), but we focus here on the changes between the two deployment years (Fig. 7). One sees that the warm season in 2004 was significantly windier than in 2003 (Figs. 7a, b). This was because in 2003 there was much greater month-to-month variability, including a period of southerly winds in July and September. This resulted in both a weaker BH and a more moderate AL. Accordingly, the anomaly shows strengthened northeasterlies in Barrow Canyon for the second year (Fig. 7c). In the cold season, the signature of the BH was similar for the first deployment year versus the second deployment year (Figs. 7d, e). The biggest difference was in the AL, which had a double-core structure during the second deployment year. However, while this led to enhanced

northerly winds in the Bering Sea and southern Chukchi Sea, there was essentially no difference in the vicinity of Barrow Canyon (Fig. 7f). These different wind patterns between the two mooring years have bearing on the upwelling investigated below.

4.2. Sea-ice cover

To describe the sea-ice cover in the Barrow Canyon region, we created a time series of ice concentration both at the mooring site near the head of the canyon and within a larger domain that encompasses the Northeast Chukchi Polynya (165–159ºW, 68.8–71.7ºN, see Fig. 1). For the second time series, we computed the median ice concentration from the grid points within the defined region. We divide the year into three seasons: the open water season when the concentration was less than 10%; the partial ice season when the concentration was between 10% and 70%; and the full ice season when the ice cover exceeded 70% (following Schulze et al., 2012). The different shading in Fig. 8 highlights the three seasons defined as such, applied to the ice concentration at the mooring position.

For the two-year period (from 1 September 2002 to 31 August 2004) at the head of Barrow Canyon, the full ice and open water seasons were roughly comparable in length, both of which were much longer than the partial ice season (Fig. 8). The variability in ice cover was considerably more pronounced at the mooring site compared to the broader polynya region (compare the solid and dashed curves). Overall, the sea ice was more highly concentrated in the winter of 2002–2003 than the winter of 2003–2004, and the full ice season lasted two weeks longer the first deployment year. Furthermore, in winter of 2003–2004 there were more openings during the full ice period (five openings compared to two during winter 2002–2003). The model simulations of Kawaguchi et al. (2011) show that the polynya adjacent to the Alaska coast tends to occur more frequently when the AL is in the northwestern part of the Bering Sea across the western Aleutian Islands. This was indeed the case for winter season 2003–2004 (Fig. 7e), although no substantial difference in the wind field over the polynya region was evident between the two winter seasons (Fig. 7f). The role of sea ice in upwelling is investigated below in section 5.2.

5. Upwelling events at the head of Barrow Canyon

In this section, we examine the characteristics and variability of the wind-induced upwelling at the head of Barrow Canyon using the near-bottom mooring data. We then consider the influence of the atmospheric forcing and sea-ice cover.

5.1. General characteristics of upwelling

5.1.1. Upwelling criteria

Past studies along the Beaufort and Chukchi slopes have identified upwelling based on a set of criteria (e.g. Pickart et al., 2009; Schulze and Pickart, 2012; Lin et al., 2018). The first requirement is that the winds are upwelling favorable, the second is that the flow along the shelfbreak is reversed (i.e. directed westward), and the third is that anomalously dense water appears near the bottom in the vicinity of the shelfbreak (having been advected upslope from the basin). In the present study, we have removed the third requirement. The rationale is that, at certain times of the year, the water at the head of Barrow Canyon is denser than that offshore of the canyon at similar depths or deeper. In these instances, the upwelled water could in fact be less dense than the water previously residing at the head. As such, we have identified upwelling events as those periods when there is a flow reversal (southward flow) at the mooring position stronger than 10 cm s^{-1}, coincident with northerly winds. If two flow reversals were not separated in time by more than 12 hours, they are considered one event. The results are not sensitive to the precise choice of the flow reversal threshold.

5.1.2. Characteristics of upwelling

Over the two-year study period (August 2002 to September 2004) there were a total of 54 upwelling events meeting the above criteria – 27 in each deployment year. Of these events, 33 were associated with denser water observed at the mooring site and 21 had lighter water present at the site (shown by the black and white bars, respectively, in Fig. 5). The potential density anomaly was computed relative to the density observed at the beginning of the current reversal. The majority of the events having negative density anomaly occurred during the cold season (October–March, 16 events). This is consistent with the fact that the Chukchi Shelf is predominantly filled with winter water modes (WW and HSWW), denser than the ambient water offshore, during winter. Another scenario resulting in a negative density anomaly at the mooring site occurs when a previous upwelling event has advected AW onto the shelf. After the wind subsides the AW starts draining northwards out of the canyon, and if this process is not complete by the time of the following event

403 then lighter water can appear at the head of the canyon. Both cases are evident in Fig. 5. For
404 example, the former scenario was observed in January 2003, and the latter in mid-November 2002.
405
406 Schulze and Pickart (2012) identified 45 wind-driven upwelling events (shown by the red
407 bars on Fig. 5) on the Beaufort shelfbreak/slope, using mooring data collected during the same time
408 as our study, roughly 150 km to the east of Barrow Canyon. Our analysis demonstrates that 40 out
409 of the 45 Beaufort slope events coincided with upwelling at the head of Barrow Canyon. The
410 percentage likely would have been larger, but four of the Beaufort slope events occurred during
411 summer 2003, when we had no velocity data in Barrow Canyon. Furthermore, the fifth event was
412 preceded by particularly strong northward flow out of the canyon, which was strongly retarded but
413 not reversed. This suggests that upwelling on the Beaufort slope is nearly always associated with
414 upwelling in Barrow Canyon.
415
416 On the other hand, 9 of 54 upwelling events identified in the canyon were not coincident
417 with upwelling on the Beaufort slope (which is not due to missing data). Several things might
418 explain this difference. For example, shelf waves are known to cause flow reversals in the canyon
419 (e.g. Aagaard and Roach, 1990; Danielson et al., 2014). However, we argue that the main factor is
420 the atmospheric forcing. To demonstrate this, we constructed composite fields using the reanalysis
421 data for the cases when upwelling occurred at both sites versus only in Barrow Canyon (Fig. 9). In
422 the former case, there is a well-developed Beaufort High and Aleutian Low which result in
423 northeasterly winds. By contrast, in the latter case the AL is displaced more to the east and there is
424 no signature of the BH. Instead, high pressure resides over Siberia and the resulting east-to-west
425 SLP gradient leads to more northerly winds – which are not conducive for upwelling along the
426 Beaufort slope.
427
428 The mean up-canyon velocity for all the upwelling events was ~30 cm s^{-1}, while the
429 strongest velocities observed exceeded 120 cm s^{-1}. The average length of an upwelling event was 70
430 hours, varying from 14 to 169 hours. The longest upwelling events occurred during early February
431 in both years. Seasonally, the greatest number of events occurred in winter (Dec–Feb, 20 events),
432 followed by fall (Sep–Nov, 17 events), spring (Mar–May, 14 events), and summer (Jun–Aug, 3
433 events). It should be remembered that during summer 2003 there were no velocity data, hence no
434 upwelling events could be identified. The good correspondence with upwelling events on the
435 Beaufort Slope suggests that there could have been four additional flow reversals, driven by
436 northeasterly winds that summer. The enhanced frequency of upwelling in late-fall to early-winter
437 recorded here is consistent with the observations of Aagaard and Roach (1990) in Barrow Canyon.
438 While Pickart et al. (2013) found two seasonal peaks in the occurrence of upwelling along the

Beaufort slope, in May and November, we did not observe a comparable seasonality. This could be because Pickart et al. (2013) used longer time series. However, while there is a strong springtime peak in easterly winds in the region, which is conducive for upwelling along the Beaufort slope (Lin et al., 2016), Fig. 4b indicates that the component of wind along the axis of Barrow Canyon in our study period in fact decreases from February into spring.

To evaluate the time delay between the onset of northerly winds and reversed up-canyon flow, we calculated the correlation between the rotated wind and along-canyon velocity. The resulting wind-current time lag of 9 hours is a bit longer than that calculated by Schulze and Pickart (2012) for the shelfbreak of the Alaskan Beaufort Sea (8 hours). This is also evident in Fig. 5 where one sees that the upwelling events on the Beaufort slope commence a bit earlier than the corresponding reversals in Barrow Canyon (compare the timing of the black and white patches with that of the red patches). This could again be due to the different orientation of the bathymetry versus the winds at the two sites. One should also remember, however, that our mooring is situated near the head of the canyon, i.e. it presumably takes longer for water from the basin to transit the ~150 km distance from the mouth of Barrow Canyon to the mooring, versus the short distance from the basin to the Beaufort shelfbreak.

5.1.3. Water masses during upwelling

What water masses were upwelled to the head of Barrow Canyon during the two-year period? To examine this, we tabulated the T/S characteristics of the water present at the peak of each upwelling event, where the peak is defined as the time of maximum or minimum potential density anomaly, depending on whether the up-canyon flow advected heavier or lighter water, respectively. Note that this represents the densest or lightest water masses brought up from the basin during an event (while other water masses often preceded the appearance of the final water mass). Based on this measure, six of the seven previously discussed water masses were upwelled during the two-year period, the only exception being ACW (Fig. 10). Pickart et al. (this issue) also noted an absence of ACW during upwelling events using full water column data from the central portion of Barrow Canyon. In Fig. 10 we divide the results into the cold and warm seasons. This reveals that there were many more events during the cold season (37) than in the warm season (17). The timing of the events is also marked on the time series of the water masses in Fig. 5, highlighting how rare upwelling was in summer.

Consider first the densest water mass upwelled to the mooring site, the AW. Previous studies have noted the presence of AW on the Chukchi Shelf to the south of Barrow Canyon (e.g. Bourke and Paquette, 1976), but, according to Weingartner et al. (2005), it is rarely advected farther than

475 Icy Cape. During our two-year study period, AW was upwelled to the mooring site only during the
476 cold season. This is consistent with earlier measurements (Mountain et al., 1976; Bourke and
477 Paquette, 1976; Aagaard and Roach, 1990; Weingartner et al., 1998). In a study of upwelling on the
478 Beaufort slope, Lin et al. (2018) found that, under the same wind conditions, Pacific-origin water
479 was primarily upwelled during the summer months, while AW was upwelled more frequently
480 during the remainder of the year. They argued that this is due to seasonal variations in the wind
481 stress curl offshore of the continental slope that causes the Pacific Water/Atlantic Water interface to
482 migrate vertically in the water column. In summer, the interface is depressed, making the AW less
483 accessible. This could explain why we only observed AW being upwelled during the cold season
484 (we note that all of the AW upwelling events were positive density anomaly events).
485
486 During the warm season, all the upwelling events at the mooring site were associated with
487 Pacific Water. Furthermore, 11 of the 14 events were associated with newly ventilated winter water
488 (WW or HSWW, Fig. 10). As seen in Figs. 4 and 5, WW first starts appearing at the mooring site in
489 December and is observed intermittently until the end of August/early September. Pickart et al. (this
490 issue) also observed WW in the canyon during August and September in a collection of repeat
491 hydrographic sections crossing the middle of the canyon, spanning a four-year period. This is
492 consistent with the seasonal presence of this water mass within the interior flow paths of the
493 Chukchi Shelf that deliver the dense water to the canyon. As such, WW should occupy the region
494 seaward of Barrow canyon as it exits into the basin during (and shortly after) this time frame, which
495 would make it readily available for upwelling during northeasterly wind events. Both positive and
496 negative density anomaly events were associated with different types of winter water.
497
498 The other two Pacific-origin water masses present at the head of Barrow Canyon during the
499 peak of upwelling events were RWW and BSW (Fig. 10). The former was measured mostly in the
500 cold season (there were only two events during warm season) mainly in the first half, as opposed to
501 the late-winter to early-spring occurrences of WW. BSW was observed only once (late-November
502 2003), also during the cold season. The lightest water mass upwelled to the head of Barrow Canyon
503 was the Arctic-origin MW. One event occurred in November 2003 (Fig. 10), associated with a
504 positive density anomaly (although the magnitude of the anomaly was small). This was during a
505 period of three consecutive northerly storms, and hence sustained wind mixing might have brought
506 the MW to depth (this water mass is normally found in the surface layer).
507
508 The above results pertain to the peak of the upwelling. It is of interest as well to determine
509 the full suite of water masses that are advected past the mooring site during upwelling. More than
510 80% of the water measured during upwelling events over the two-year period was winter water:

WW (~44.4%), RWW (~34%), and a small amount of HSWW (~5.2%). Thus, most upwelling events in Barrow Canyon resulted in the reintroduction of cold Pacific Water onto the shelf. Notably, the WW and HSWW are both very high in nitrate (e.g. Lowry et al., 2015), which could help explain the enhanced biological productivity observed in the canyon (Grebmeier et al., 2015). The next most common water mass was AW (~9.4%) followed by BSW (~5.4%). The percentage of the two lightest water masses, ACW (~0.4%) and MW (~1.2%), were negligibly small.

This may seem at odds with the results of Lin et al. (2018) who observed little-to-no Pacific Water upwelling events on the Beaufort slope during the cold months based on 6 years of mooring data. Overall, they found that AW was upwelled three times more frequently than Pacific Water. Here we find the opposite trend – only 5 out of the 54 events contained AW at their peaks. This is most likely due to the difficulty of drawing such dense AW all the way from the basin to the head of the canyon, which was also noted by Aagaard and Roach (1990). The seasonal trends found by Lin et al. (2018) may apply more closely to the canyon mouth.

5.2. Atmospheric forcing

5.2.1. Large-scale circulation

We now investigate the atmospheric circulation patterns that resulted in the upwelling during the study period. Following the analysis in Section 4.1, we consider the warm months (April–September) and the cold months (October–March). We created composite maps of SLP and 10 m winds for the times in which upwelling was occurring versus the non-forced periods for these two times of the year (Fig. 11).

One sees that, during the warm months, upwelling took place when the Beaufort High was well developed and there was a signature of the Aleutian Low in the Bering Sea (Fig. 11a). This is similar to the findings of Weingartner et al. (2017) and Pickart et al. (this issue) who considered upwelling in Barrow Canyon in more recent years. For the unforced periods during the warm months, there are only weak signatures of these two centers of action and very light winds in the canyon (Fig. 11b). During the cold months, the upwelling in Barrow Canyon is also driven by the Beaufort High in conjunction with the Aleutian Low (Fig. 11d). However, both centers of action have stronger signatures compared with the warm season composite. This is to be expected because, as shown above, climatologically the BH is stronger in winter and the AL is deeper (Fig. 6). This is also seen in the unforced composite for the cold months of our study period (Fig. 11e). The anomaly fields reveal that, while both centers of action change considerably during upwelling in the warm period, it is primarily the AL that is altered (deepened) when upwelling occurs during the

cold months (compare Figs. 11c and f). Pickart et al. (2009) found this to be true as well for upwelling along the Beaufort slope.

5.2.2. Strength of forcing versus water column response

Over the two-year period there was a wide range of up-canyon wind speeds that resulted in upwelling. To document this, we tabulated the number of upwelling events identified from the mooring time series as a function of wind speed threshold (Fig. 12). The strongest forcing was 16 m s^{-1} (one event), while the weakest was 5 m s^{-1} (two events). This distribution of wind events is similar to that previously reported for the Beaufort slope. Using data over the same two-year period considered here, Schulze and Pickart (2012) determined that upwelling commences on the Beaufort slope once the easterly wind speed exceeds 4 m s^{-1}. Based on 6 years of mooring data at the same location (2008–13), Lin et al. (2016) constructed a composite upwelling event based on 131 individual events. They determined that the average peak wind speed was between 5–6 m s^{-1}.

Do the strongest up-canyon wind speeds result in the strongest upwelling events in Barrow Canyon? To assess this, it was necessary to define a robust measure of the strength of forcing as well as the strength of the water column response. For the former, we followed Pisareva et al. (2015) and used the Barrow meteorological data to compute the time integral of the wind stress over each up-canyon wind event (whether or not the event resulted in upwelling),

$$I_w = \int_{t_{ws}}^{t_{we}} |\tau_a(t)| dt, \qquad (1)$$

where τ_a is the along-canyon component of the wind stress (computed following Large and Pond, 1981), and t_{ws} and t_{we} are the start and end times of the wind events. A wind event was defined when there was an up-canyon wind for more than 6 hours. If two events were not separated in time by more than 6 hours, those events were considered as one. Note that I_w takes into account both the magnitude of the wind as well as the length of the event. It is related to the cumulative Ekman transport defined by Huyer et al. (1979) (the cumulative Ekman transport is $I_w/\rho f$, where ρ is the density of the water and f is the Coriolis parameter).

The value of I_w for each up-canyon wind event over the two-year mooring deployment is shown in Fig. 13a, where the black squares indicate the mean for each month (the storms that occurred during summer 2003 are not included since we have no velocity data for that time period). Overall, this measure of storm strength displays the same seasonal pattern as the wind magnitude (compare Figs. 13a and 3b), with larger I_w, and larger variability, from mid-fall through mid-spring. In Fig. 13a we have marked those wind events that caused upwelling (red symbols). A clear relationship is evident: out of the 33 northerly storms with I_w greater than 0.2 N m^{-2} d, only 6 did

not induce upwelling, and all but one with I_w > 0.3 N m^{-2} d resulted in upwelling (the exception was the event in May 2004 when a strong northerly wind caused the flow in the canyon to retard but not reverse). Eight storms resulted in multiple (two, three or four) upwelling events at the head of Barrow canyon, due to the long duration of the enhanced winds. Those events are plotted overlaying each other and circled on Fig. 13a. Seven of these storms had I_w > 0.3 N m^{-2} d. At the same time, our data suggest that it is not necessary for a wind event to have I_w greater than some threshold to cause upwelling. As seen in Fig. 13, six of the upwelling events had I_w < 0.1 N m^{-2} d.

The seasonal distribution of I_w for all the wind events over the period 1979–2014 (corresponding to the NARR coverage) displays a similar pattern as the two-year period of our study (Fig. 13b). Storms tend to be weaker in the summer months with less variability. Based on our two-year mooring data set, 82% of the wind events with I_w > 0.2 N m^{-2} d resulted in upwelling. Consequently, we can extrapolate and conclude that there were at least 428 upwelling events at the head of Barrow Canyon over the 36-year period (also keep in mind, that a single storm can force multiple flow reversals in the canyon).

To determine the strength of the upwelling response, Lin et al. (2016) calculated an upwelling index that considers both the duration of the event and the magnitude of the resulting density anomaly. As discussed earlier, we are considering both positive and negative density anomaly events. As such, we use a metric based on the strength and duration of the reversed flow at the head of the canyon, which we refer to as the flow reversal index (FRI, m s^{-1} d),

$$\mathrm{FRI} = \int_{t_{us}}^{t_{ue}} |U(t)|\, dt, \qquad (2)$$

where U is the magnitude of the along-canyon flow reversal measured by the mooring, and t_{us}, t_{ue} are start time and end time of each upwelling event (defined as the start and the end of a flow reversal). Lin et al. (2018) found a statistically significant linear relationship between their upwelling index and the cumulative Ekman transport ($I_w/\rho f$); i.e. stronger storms tend to result in stronger upwelling. We find a similar result here. We regressed FRI against I_w for each upwelling event, where I_w was computed over the period of the flow reversal. The result is shown in Fig. 14 which reveals a statistically significant relationship (R=0.79). One might expect that the largest values of FRI would be associated with AW appearing at the mooring site (i.e. water being drawn from deeper in the basin). However, there does not appear to be a direct dependence between the value of FRI and the occurrence of AW: while three of the strongest events indeed brought AW to the head of the canyon, the other AW events had much smaller FRI values (Fig. 14). This is not surprising in light of the results of Lin et al. (2018) who demonstrated that the primary factor

616 dictating whether or not AW is upwelled onto the Beaufort shelf is the interface height between the
617 Pacific Water and Atlantic Water in the adjacent basin.
618
619 *5.2.3. Impact of ice cover*
620 Out of the 54 events, 14 occurred during the open water period, 10 during partial ice, and 30
621 during full ice cover (Fig. 8). These percentages are comparable to those for the Beaufort slope for
622 the same time period (Schulze and Pickart, 2012), where the largest number of upwelling events
623 also occurred during full ice cover. We note that only three events brought lighter water to the
624 canyon head during the open water and partial ice seasons, while 18 such events occurred during
625 full ice season. To determine if the ice concentration impacts the upwelling response, we calculated
626 individual regressions of FRI and I_w using the data for each ice season separately. There were no
627 significant differences, implying that, to first order, ice concentration does not influence the strength
628 of the flow reversals. This is different than on the Beaufort slope where Schulze and Pickart (2012)
629 found that the upwelling response varies significantly with ice cover.
630
631 Is there a relationship between the upwelling in the canyon and the occurrence of the
632 Northeast Chukchi Polynya? To address this, first we computed the ice concentration anomaly
633 within the red box in Fig. 1. This is defined as the difference between the spatially averaged
634 concentration for a given day and the monthly average. We considered the months of December to
635 March (when ice cover is extensive on the Chukchi Shelf). As discussed above, a value of I_w greater
636 than 0.3 N m^{-2} d implies that upwelling is occurring in the canyon. Using this threshold, we were
637 able to consider a longer time period for the analysis (2002–2017).
638
639 For each month, we tabulated the number of days in the month that the ice concentration
640 anomaly was negative, and compared this to the number of upwelling days during the month. This
641 revealed a clear relationship such that more upwelling days are associated with less ice in the
642 polynya region (Fig. 15). We also considered all the storms (i.e. relaxing the threshold for I_w) and
643 found that, while there is a significant relationship, the correlation is weaker (R = 0.58 versus 0.79).
644 In addition, we singled out the polynya events as those instances when the average concentration in
645 the box fell below 85%. This resulted in nearly the same relationship as in Fig. 15. The slope of the
646 regression in Fig. 15 implies that roughly 50% of the upwelling days correspond to a negative ice
647 anomaly in the polynya region. The main reason that the percentage is not larger is that there is a
648 delay in the ice response south of the canyon to the onset of the upwelling favorable winds. This
649 was demonstrated by compositing all the events over the 15-year period and quantifying the
650 relationship between the upwelling winds and the anomaly in ice cover.

We note that the Northeast Chukchi Polynya has been classified as a hybrid sensible-heat/wind-driven polynya, meaning that it is formed by wind-driven divergence and also influenced by the upwelling of warm AW onto the shelf, which can melt ice (Ladd et al., 2016; Hirano et al., 2016). Interestingly, two upwelling events during the second deployment year, that coincided with substantial openings in the ice, brought Atlantic Water to the head of the canyon (Fig. 8) and had the largest values of FRI (Fig. 14). However, while our results do not distinguish between wind forcing versus ice melt, only 5 of the 54 upwelling events in our two-year mooring record brought AW to the head of the canyon. This implies that wind forcing is the dominant influence on the formation of the polynya.

6. Summary

Using two years of mooring observations from the head of Barrow Canyon, together with atmospheric and ice concentration data, we investigated the seasonal signals in the canyon as well as aspects of upwelling and the wind-forcing that drives it. While previous studies have addressed upwelling in Barrow Canyon using moored data (e.g. Weingartner et al., 2017), much of our focus was on the individual events that occurred over a two-year period. This allowed us to perform a detailed analysis of the water masses brought to the head of the canyon and how this relates to the strength of the wind-driven flow reversals. As such, we have provided valuable insights into the nature of upwelling in Barrow canyon, which is critical for improving our understanding of local biological responses to this physical variability.

On average, the flow in Barrow Canyon over the two-year study period was down-canyon during each month of the year except February, when the up-canyon winds were strongest. During the summer months, most of the deep water at the canyon head consisted of newly ventilated winter water (WW) and remnant winter water (RWW), consistent with the seasonal delivery of these dense water masses to the canyon via interior shelf pathways. During the fall, both summer Pacific-origin water masses, Bering Summer Water (BSW) and Alaskan Coastal Water (ACW), were present while Atlantic Water (AW) was measured as well due to upwelling activity. The winter and spring seasons were characterized by the largest volumes of dense winter water, including hypersaline winter water (HSWW) near the freezing point. Overall, nearly 80% of the deep flow through the head of the canyon during the two-year period consisted of cold and dense winter waters.

Different mechanisms are known to cause upwelling in the canyon, including propagation of shelf-edge waves and changes in the meridional sea level pressure gradient. We considered only wind-driven upwelling events, which dominated the record. The events were identified as periods of flow reversals (i.e. up-canyon flow) associated with northeasterly winds. Unlike the Beaufort shelf/slope, where upwelling always advects denser water to the vicinity of the shelfbreak, in Barrow Canyon the flow reversals at times deliver lighter water to the head of the canyon. Of the 54 identified upwelling events, 33 were associated with a positive near-bottom density anomaly at the head of the canyon, while 21 resulted in lighter waters at the site. The latter scenario largely occurred during the cold season due to the generally homogeneous T/S conditions (the canyon was already filled with heavy winter water modes). Most of the events measured in the canyon coincided with upwelling on the Beaufort slope. The exceptions occurred during northerly winds (versus northeasterly) due to the positions of the Aleutian Low and Siberian High.

Over the two-year mooring deployment, all the Pacific-origin water masses were upwelled to the head of the canyon except for ACW. In the warm season, most of the events consisted of WW or HSWW because these dense water masses have only recently exited the canyon at this time of the year. AW was upwelled to the mooring site only during the cold season, consistent with observations on the Beaufort slope, demonstrating that this water mass is more accessible in the adjacent basin during these months (see Lin et al., 2018). Overall, the majority of upwelling events in Barrow Canyon resulted in the reintroduction of cold Pacific Winter Water onto the shelf, rather than advection of AW. This is in contrast to the Beaufort slope where upwelling of AW is far more common. This is likely because of the long distance that the AW has to travel to reach the head of the canyon. Notably, the high-nutrient winter water is conducive for enhanced productivity, which in turn may help explain why Barrow Canyon is associated with high benthic biomass and increased numbers of marine mammals and seabirds.

Overall, we observed more than twice as many upwelling events during the cold season as the warm season due to the seasonal enhancement of upwelling-favorable winds. By constructing composite atmospheric fields using reanalysis data, we demonstrated that upwelling in Barrow Canyon occurs when the Beaufort High is strong and the Aleutian Low is deep, consistent with the previous study of Weingartner et al. (2017). These conditions are also conducive for enhanced offshore ice transport and polynya openings along the Alaskan coast (Hirano et al., 2017), which is evident in our data as well. Danielson et al. (2014) found that when the Aleutian Low is centered over the Bering Sea it tends to cause coastal convergence along the Alaskan coast, resulting in northward propagating shelf waves. Further investigation is necessary to elucidate the precise relationship between upwelling in Barrow Canyon and the large-scale atmospheric patterns, continental shelf waves, and variations of the Pacific-Arctic sea level gradient.

We quantified the strength of the atmospheric forcing by computing the time integral of the wind stress, I_w, during all the up-canyon wind events. The magnitude and variability of I_w were considerably smaller in the summer compared with the rest of the year. To relate the wind forcing to the water column response, we defined a flow reversal index (FRI) which takes into account both the duration and magnitude of the up-canyon velocity. We found that there was a statistically significant relationship between I_w and FRI such that stronger storms tend to result in stronger upwelling, similar to the case for the Beaufort slope (Lin et al., 2018). In contrast to the Beaufort slope, however, the strength of the upwelling response does not appear to be impacted by the presence of ice cover. The reasons for this warrant further investigation. Finally, it was demonstrated that upwelling typically corresponds with the occurrence of the Northeast Chukchi Polynya.

Acknowledgments

The authors would like to thank the SBI scientific team and the crews of the USCGC *Polar Star* and *Healy*. Carolina Nobre provided the software for identifying the upwelling events, and K. Moore provided the NARR data. Seth Danielson quality controlled the Barrow wind time series. We also thank the anonymous reviewers whose insightful comments led to improvements in the paper. RP was funded under grant PLR-1303617 and ARC-1203906 from the National Science Foundation. PL was funded under grant NA14-OAR-4320158 from the National Oceanic and Atmospheric Administration. The paper was written in the framework of the state assignment of FASO Russia (theme No. 0149-2019-0004).

References

Aagaard, K. and A.T. Roach, 1990. Arctic ocean-shelf exchange: Measurements in Barrow Canyon. J. Geophys. Res.: Oceans, 95(C10), 18163-18175. https://doi.org/10.1029/JC095iC10p18163.

Bourke, R.H. and R.G. Paquette, 1976. Atlantic water on the Chukchi shelf. Geophys. Res. Lett. 3, 629–632. https://doi.org/10.1029/GL003i010p00629.

Brugler, E.T., R.S. Pickart, G.W.K. Moore, S. Roberts, T.J. Weingartner and H. Statscewich, 2014. Seasonal to interannual variability of the Pacific water boundary current in the Beaufort Sea. Prog. Oceanogr., 127, 1–20. https://doi.org/10.1016/j.pocean.2014.05.002.

Carmack, E. C., and E. A. Kulikov, 1998. Wind-forced upwelling and internal Kelvin wave generation in Mackenzie Canyon, Beaufort Sea, J. Geophys. Res.: Oceans, 103, 18,447–18,458. https://doi.org/10.1029/98JC00113.

Cavalieri, D. J., J. P. Crawford, M. R. Drinkwater, D. T. Eppler, L. D. Farmer, R. R. Jentz, and C. C. Wackerman, 1991. Aircraft active and passive microwave validation of sea ice concentration from the Defense Meteorological Satellite Program special sensor microwave imager. J. Geophys. Res.: Oceans, 96(C12), 21989–22008. https://doi.org/10.1029/91JC02335.

Coachman, L.K., K. Aagaard and R.B. Tripp, 1975. Bering Strait, The Regional Physical Oceanography. University of Washington Press, Seattle and London, p.172.

Codispoti, L., C. Flagg, V. Kully, and J. H. Swift, 2005. Hydrographic conditions during the 2002 SBI process experiments. Deep-Sea Res., II, 52 (24-26): 3199 – 3226. http://dx.doi.org/10.1016/j.dsr2.2005.10.007.

Cooper, L.W., T.E. Whitledge, J.M. Grebmeier and T.J. Weingartner, 1997. The nutrient, salinity, and stable oxygen isotope composition of Bering and Chukchi Seas waters in and near the Bering Strait. J. Geophys. Res.: Atmospheres, 1021(C6): 12563-12574. https://doi.org/10.1029/97JC00015.

Corlett, W.B., and R. S. Pickart, 2017. The Chukchi Slope Current. Prog. Oceanogr., 153, pp. 50-65. https://doi.org/10.1016/j.pocean.2017.04.005.

Danielson, S., T. Weingartner, K. Hedstrom, K. Aagaard, R. Woodgate, E. Curchitser, and P. Stabeno, 2014. Ekman transport, continental shelf waves, and variations of the Pacific-Arctic sea surface height gradient: Coupled wind-forced controls of the Bering-Chukchi shelf circulation and the Bering Strait throughflow. Progr. Oceanogr., 125: 40 – 61. https://doi.org/10.1016/j.pocean.2014.04.006.

Ershova, E.A., R.R. Hopcroft, K.N. Kosobokova, K. Matsuno, R.J. Nelson, A. Yamaguchi and L.B. Eisner, 2015. Long-Term Changes in Summer Zooplankton Communities of the Western Chukchi Sea, 1945–2012. Oceanography 28(3): 100-115. http://dx.doi.org/10.5670/oceanog.2015.60.

Favorite, F., 1976. Oceanography of the subarctic Pacific region, 1960–1971. Bull. Int. North Pac. Commission, 31, 1960–1971.

Gong, D. and R.S. Pickart, 2015. Summertime circulation in the eastern Chukchi Sea. Deep-Sea Res. II 118, 18–31. http://dx.doi.org/10.1016/j.dsr2.2015.02.006.

Grebmeier, J.M., S.E. Moore, J.E. Overland, K.E. Frey, and R. Gradinger, 2010. Biological response to recent Pacific Arctic sea ice retreats. Eos, Transactions American Geophysical Union 91(18):161–162. http://dx.doi.org/10.1029/2010EO180001.

Grebmeier, J.M., B.A. Bluhm, L.W. Cooper, S.L. Danielson, K.R. Arrigo, A.L. Blanchard, J.T. Clarke, R.H. Day, K.E. Frey, R.R. Gradinger, M. Kedra, B. Konar, K.J. Kuletz, S.H. Lee, J.R. Lovvorn, B.L. Norcross and S.R. Okkonen, 2015. Ecosystem characteristics and processes facilitating persistent macrobenthic biomass hotspots and associated benthivory in the Pacific Arctic. Prog. Oceanogr., 136, 92–114. https://doi.org/10.1016/j.pocean.2015.05.006.

Hill, V. and G. Cota, 2005. Spatial patterns of primary production on the shelf, slope and basin of the Western Arctic in 2002. Deep-Sea Res. II 52, 3344–3354. http://dx.doi.org/10.1016/j.dsr2.2005.10.001.

Hirano, D., Y. Fukamachi, E. Watanabe, K. I. Ohshima, K. Iwamoto, A. R. Mahoney, H. Eicken, D. Simizu, and T. Tamura, 2016. A wind-driven, hybrid latent and sensible heat coastal polynya off Barrow, Alaska. J. Geophys. Res.: Oceans, 121, 980–997. https://doi.org/10.1002/2015JC011318.

Itoh, M., S. Nishino, Y. Kawaguchi and T. Kikuchi, 2013. Barrow Canyon volume, heat, and freshwater fluxes revealed by long-term mooring observations between 2000 and 2008. J. Geophys. Res.: Oceans, 118, 4363–4379. http://dx.doi.org/ 10.1002/jgrc.20290.

Itoh, M., R.S. Pickart, T. Kikuchi, Y. Fukamachi, K.I. Ohshima, D. Simizu, K.R. Arrigo, S. Vagle, J. Heg, C. Ashjian, J.T. Mathis, S. Nishino and C. Nobre, 2015. Water properties, heat and volume fluxes of Pacific water in Barrow Canyon during summer 2010. Deep-Sea Res. I: Oceanographic Res. Papers, Volume 102, pp. 43–54. http://dx.doi.org/10.1016/j.dsr.2015.04.004.

Jakobsson, M., L. A. Mayer, B. Coakley, J. A. Dowdeswell, S. Forbes, B. Fridman, H. Hodnesdal, R. Noormets, R. Pedersen, M. Rebesco, H.-W. Schenke, Y. Zarayskaya A, D. Accettella, A. Armstrong, R. M. Anderson, P. Bienhoff, A. Camerlenghi, I. Church, M. Edwards, J. V. Gardner, J. K. Hall, B. Hell, O. B. Hestvik, Y. Kristoffersen, C. Marcussen, R. Mohammad, D. Mosher, S. V. Nghiem, M. T. Pedrosa, P. G. Travaglini, and P. Weatherall, 2012. The International Bathymetric Chart of the Arctic Ocean (IBCAO) Version 3.0, Geophys. Res. Lett., 39, L12609. https://doi.org/10.1029/2012GL052219.

Kampf, J., 2005. Cascading-driven upwelling in submarine canyons at high latitudes, J. Geophys. Res., 110, C02007. https://doi.org/10.1029/2004JC002554.

Kawaguchi, Y., T. Tamura, S. Nishino, T. Kikuchi, M. Itoh and H. Mitsudera, 2011. Numerical study of winter water formation in the Chukchi Sea: Roles and impacts of coastal polynyas. J. Geophys. Res., 116, C07025. https://doi.org/10.1029/2010JC006606.

Ladd, C., C. W. Mordy, S. A. Salo, and P. J. Stabeno, 2016. Winter Water Properties and the Chukchi Polynya. J. Geophys. Res.: Oceans, 121, 5516–5534. https://doi.org/10.1002/2016JC011918.

Large, W.G., and S. Pond, 1981. Open ocean momentum flux measurements in moderate to strong winds. J. Phys. Oceanogr., 11, 324-336. https://doi.org/10.1175/1520-0485(1981)011<0324:OOMFMI>2.0.CO;2.

Li, M., R.S. Pickart, M.A. Spall, T.J. Weingartner, P. Lin, G.W.K. Moore, and Y. Qi, 2019. Circulation of the Chukchi Sea shelfbreak and slope from moored timeseries. Prog. Oceanogr., 172, pp. 14-33. https://doi.org/10.1016/j.pocean.2019.01.002.

Lin, P., R.S. Pickart, K.M. Stafford, G.W.K. Moore, D.J. Torres, F.Bahr and J. Hu, 2016. Seasonal Variation of the Beaufort Shelfbreak Jet and its Relationship to Arctic Cetacean Occurrence. J. Geophys. Res.: Oceans, 121. https://doi.org/10.1002/2016JC011890.

Lin, P., R.S. Pickart, G.W.K. Moore, M.A. Spall and J. Hu, 2018. Characteristics and Dynamics of wind-driven upwelling in the Alaskan Beaufort Sea based on six years of mooring data. Deep-Sea Res. II. https://doi.org/10.1016/j.dsr2.2018.01.002.

Lowry, K.E., R.S. Pickart, M.M. Mills, Z.W. Brown, G.L. Dijken, N.R. Bates, and K.R. Arrigo, 2015. The influence of winter water on phytoplankton blooms in the Chukchi Sea. Deep-Sea Res. II, 118:53–72. http://dx.doi.org/10.1016/j.dsr2.2015.06.006.

Martin, T., M. Steele, and J. Zhang, 2014. Seasonality and long-term trend of Arctic Ocean surface stress in a model. J. Geophys. Res.: Oceans, 119, 1723–1738. https://doi.org/10.1002/2013JC009425.

Mesinger, F., G. DiMego, E. Kalnay, K. Mitchell, P.C. Shafran, W. Ebisuzaki, D. Jović, J. Woollen, E. Rogers, E.H. Berbery, and others, 2006. North American regional reanalysis. Bulletin of the American Meteorological Society 87(3):343–360. http://dx.doi.org/10.1175/BAMS-87-3-343.

Moore, S.E., and J.M. Grebmeier, 2018. The Distributed Biological Observatory: linking physics to biology in the Pacific Arctic region. Arctic 71, Suppl. 1, 1-7. http://doi.org/10.14430/arctic4606.

Mountain, D. G., L. K. Coachman, and K. Aagaard, 1976. On the flow through Barrow Canyon, J. Phys. Oceanogr., 6, 461–470. http://dx.doi.org/10.1175/1520-0485(1976)006<0461:OTFTBC>2.0.CO;2.

Nikolopoulos, A., R.S. Pickart, P.S. Fratantoni, K. Shimada, D.J. Torres and E.P. Jones, 2009. The western Arctic boundary current at 152 °W: Structure, variability, and transport. Deep-Sea Res. II 56, 1164–1181. https://doi.org/10.1016/j.dsr2.2008.10.014.

Pawlowicz, R., B. Beardsley, and S. Lentz, 2002. Classical tidal harmonic analysis including error estimates in MATLAB using T_TIDE. Computers and Geosciences 28, 929-937. https://doi.org/10.1016/S0098-3004(02)00013-4.

Pickart, R. S., 2004. Shelfbreak circulation in the Alaskan Beaufort Sea: Mean structure and variability. J. Geophys. Res., 109, C04024. https://doi.org/10.1029/2003JC001912.

Pickart, R.S., T.J. Weingartner, L.J. Pratt, S. Zimmermann and D.J. Torres, 2005. Flow of winter-transformed water into the western Arctic. Deep-Sea Res. II, 52, 3175–3198. https://doi.org/10.1016/j.dsr2.2005.10.009.

Pickart, R.S. and G. Stossmeister, 2008. Outflow of Pacific Water from the Chukchi Sea to the Arctic Ocean. Chinese J. of Polar Science, Vol. 19, No. 2, pp. 135-148.

Pickart, R. S., G. W. K. Moore, D. J. Torres, P. S. Fratantoni, R. A. Goldsmith, and J. Yang, 2009. Upwelling on the continental slope of the Alaskan Beaufort Sea: Storms, ice, and oceanographic response. J. Geophys. Res.: Oceans, 114, C00A13.

908 https://doi.org/10.1029/2008JC005009.
909
910 Pickart, R.S., L.J. Pratt, D.J. Torres, T.E. Whitledge, A.Y. Proshutinsky, K. Aagaard, T.A. Agnew,
911 G.W.K. Moore and H.J. Dail, 2010a. Evolution and dynamics of the flow through Herald
912 Canyon. Deep-Sea Res. II, 57 (1-2), 5–26. https://doi.org/10.1016/j.dsr2.2009.08.002.
913
914 Pickart, R.S., M.A. Spall, G.W.K. Moore, T.J. Weingartner, R.A. Woodgate, K.Aagaard and K.
915 Shimada, 2010b. Upwelling in the Alaskan Beaufort Sea: Atmospheric forcing and local
916 versus non-local response. Prog. Oceanogr., 88, 78–100.
917 https://doi.org/10.1016/j.pocean.2010.11.005.
918
919 Pickart, R.S., L.M. Schulze, G.W.K. Moore, M.A. Charette, K.R. Arrigo, G. van Dijken and S.L.
920 Danielson, 2013. Long-term trends of upwelling and impacts on primary productivity in the
921 Alaskan Beaufort Sea. Deep-Sea Res. I, 79, 106–121.
922 https://doi.org/10.1016/j.dsr.2013.05.003.
923
924 Pickart, R.S., G.W.K. Moore, Chongyuan Mao, F. Bahr, C. Nobre and T.J. Weingartner, 2016.
925 Circulation of winter water on the Chukchi shelf in early Summer. Deep-Sea Res. II, 130,
926 56–75. http://dx.doi.org/10.1016/j.dsr2.2016.05.001.
927
928 Pickart, R.S., C. Nobre, P. Lin, K.R. Arrigo, C.J. Ashjian, C. Berchok, L.W. Cooper, J.M.
929 Grebmeier, I. Hartwell, J. He, M. Itoh, T. Kikuchi, S. Nishino and S. Vagle. Seasonal to
930 mesoscale variability of water masses and atmospheric conditions in Barrow Canyon,
931 Chukchi Sea. Deep-Sea Res. II, (this issue).
932
933 Pisareva, M.N., R.S. Pickart, M.A. Spall, C. Nobre, D.J. Torres, G.W.K. Moore and T.E.
934 Whitledge, 2015. Flow of pacific water in the western Chukchi Sea: Results from the 2009
935 RUSALCA expedition. Deep-Sea Res. I, 105, 53–73.
936 https://doi.org/10.1016/j.dsr.2015.08.011.
937
938 Reynolds, R.W., T.M. Smith, C. Liu, D.B. Chelton, K.S. Casey and M.G. Schlax, 2007. Daily high-
939 resolution-blended analyses for sea surface temperature. J.Clim. 20 (22), 5473–5496.
940 http://dx.doi.org/10.1175/2007JCLI1824.1.
941
942 Rudels, B., E.P. Jones, U. Schauer and P. Eriksson, 2004. Atlantic sources of the Arctic Ocean
943 surface and halocline waters. Polar Res. 23, 181–208. https://doi.org/10.1111/j.1751-
944 8369.2004.tb00007.x.
945
946 Schulze, L.M. and R.S. Pickart, 2012. Seasonal variation of upwelling in the Alaskan Beaufort Sea:
947 Impact of sea ice cover. J. Geophys. Res.: Oceans, 117, C06022.
948 https://doi.org/10.1029/2012JC007985.
949
950 Shimada, K., T. Kamoshida, M. Itoh, S. Nishino, E. Carmack, F. McLaughlin, S. Zimmermann and
951 A. Proshutinsky, 2006. Pacific Ocean inflow: Influence on catastrophic reduction of sea ice
952 cover in the Arctic Ocean. Geophys. Res. Lett., 338.
953 https://doi.org/10.1029/2005GL025624.
954
955 Shroyer, E. L., 2012. Turbulent kinetic energy dissipation in Barrow Canyon. J. Phys. Oceanogr.,
956 42, 1012-1021. http://dx.doi.org/10.1175/JPO-D-11-0184.1.
957
958 Shroyer, E. L. and R.S. Pickart, accepted. Pathways, timing, and evolution of Pacific Winter Water
959 through Barrow Canyon. Deep-Sea Res. II, (this issue).
960

961 Spall, M.A., R.S. Pickart, P.S. Fratantoni and A.J. Plueddemann, 2008. Western Arctic shelfbreak
962 eddies: formation and transport. J. Phys. Oceanogr., 38, 1644–1668.
963 https://doi.org/10.1175/2007JPO3829.1.
964
965 Steele, M., J. Morrison, W. Ermold, I. Rigor and M. Ortmeyer, 2004. Circulation of summer Pacific
966 halocline water in the Arctic Ocean. J. Geophys. Res., 109 (C02027).
967 http://dx.doi.org/10.1029/2003JC002009.
968
969 Timmermans, M.-L., A. Proshutinsky, E. Golubeva, J. M. Jackson, R. Krishfield, M. McCall, G.
970 Platov, J. Toole, W. Williams, T. Kikuchi and S. Nishino, 2014. Mechanisms of Pacific
971 Summer Water variability in the Arctic's Central Canada Basin. J. Geophys. Res.: Oceans,
972 119, 7523–7548. https://doi.org/10.1002/2014JC010273.
973
974 Watanabe, E., 2011. Beaufort shelf break eddies and shelf-basin exchange of Pacific summer water
975 in the western Arctic Ocean detected by satellite and modeling analyses. J. Geophys. Res.,
976 116, C08034. https://doi.org/10.1029/2010JC006259.
977
978 Weingartner, T.J., D.J. Cavalieri, K. Aagaard and Y. Sasaki, 1998. Circulation, dense water
979 formation, and outflow on the northeast Chukchi shelf. J. Geophys. Res. 103, 7647–7661.
980 https://doi.org/10.1029/98JC00374.
981
982 Weingartner, T.J., K. Aagaard, R. Woodgate, S. Danielson, Y. Sasaki, and D. Cavalieri, 2005.
983 Circulation on the north central Chukchi Sea shelf. Deep-Sea Res., II, 52, 3150–3174.
984 https://doi.org/10.1016/j.dsr2.2005.10.015.
985
986 Weingartner, T.J., R.A. Potter, C.A. Stoudt, E.L. Dobbins, H. Statscewich, P.R. Winsor, T. Mudge
987 and K.Borg, 2017. Transport and thermohaline variability in Barrow Canyon on the
988 Northeastern Chukchi Sea Shelf. J. Geophys. Res.: Oceans, 122, 3565-3585.
989 https://doi.org/10.1002/2016JC012636.
990
991 Woodgate, R. A., K. Aagaard, and T. J. Weingartner, 2005a. Monthly temperature, salinity, and
992 transport variability of the Bering Strait through flow. Geophys. Res. Lett., 32, L04601.
993 https://doi.org/10.1029/2004GL021880.
994
995 Woodgate, R.A., K. Aagaard, J.H. Swift, K.K. Falkner and W.M. Smethie Jr., 2005b. Pacific
996 ventilation of the Arctic Ocean's lower halocline by upwelling and diapycnal mixing over
997 the continental margin. Geophys. Res. Lett., 32, L18609.
998 https://doi.org/10.1029/2005GL023999.
999
1000 Woodgate, R.A., T.J. Weingartner and R. Lindsay, 2012. Observed increases in Bering Strait
1001 oceanic fluxes from the Pacific to the Arctic from 2001 to 2011 and their impacts on the
1002 Arctic Ocean water column. Geophys. Res. Lett. 39, L24603.
1003 http://dx.doi.org/10.1029/2012GL054092.
1004
1005 Wood, K.R., J. Wang, S.A. Salo and P.J. Stabeno, 2015. The climate of the Pacific Artctic during
1006 the first RUSALCA decade: 2004-2013. Oceanography 28(3): 24–35.
1007 http://dx.doi.org/10.5670/oceanog.2015.55.
1008

Figures

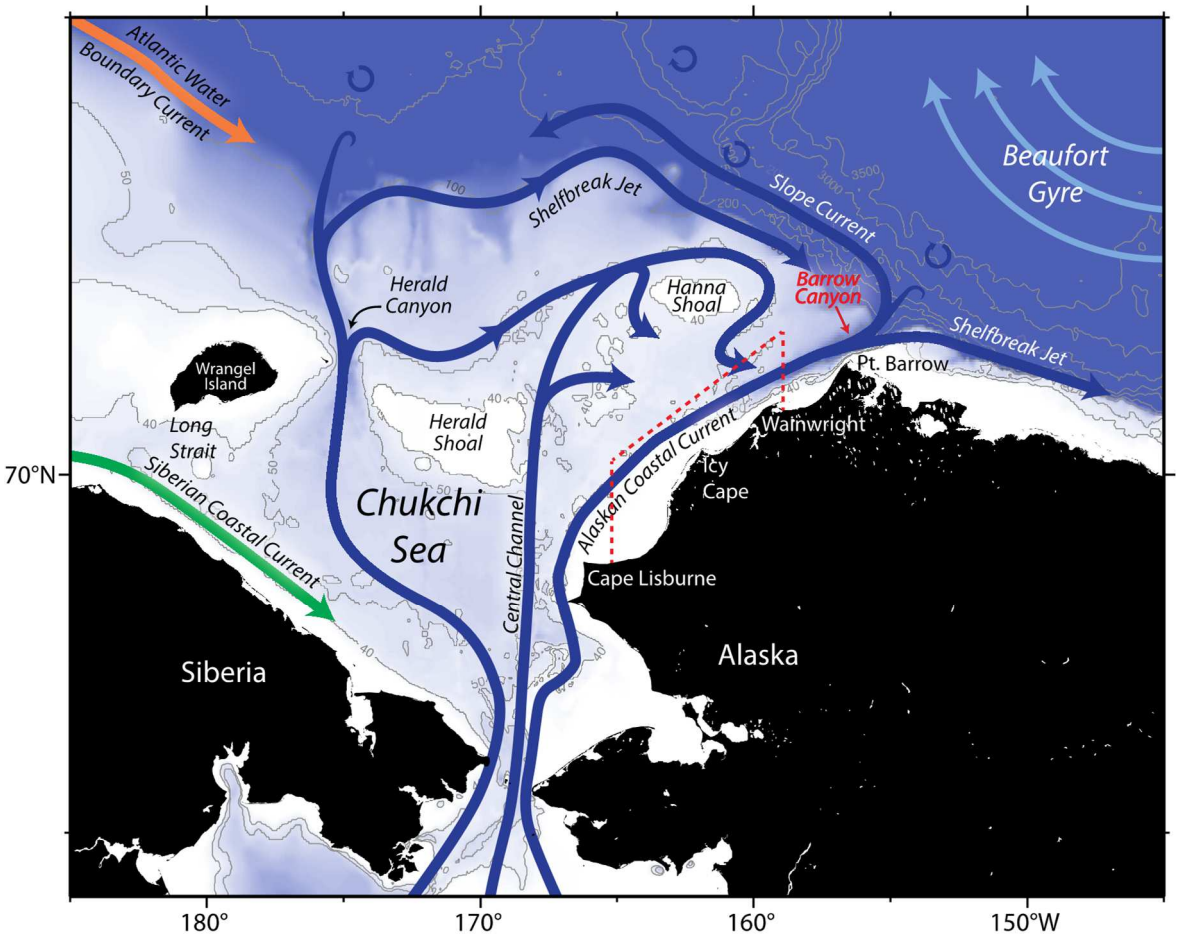

Fig. 1. Schematic circulation of Pacific-origin water in the Chukchi Sea and geographical place names (adopted from Corlett and Pickart, 2017). The polynya box in the northeast part of the shelf, discussed in Section 4.2, is delimited by the dashed red line.

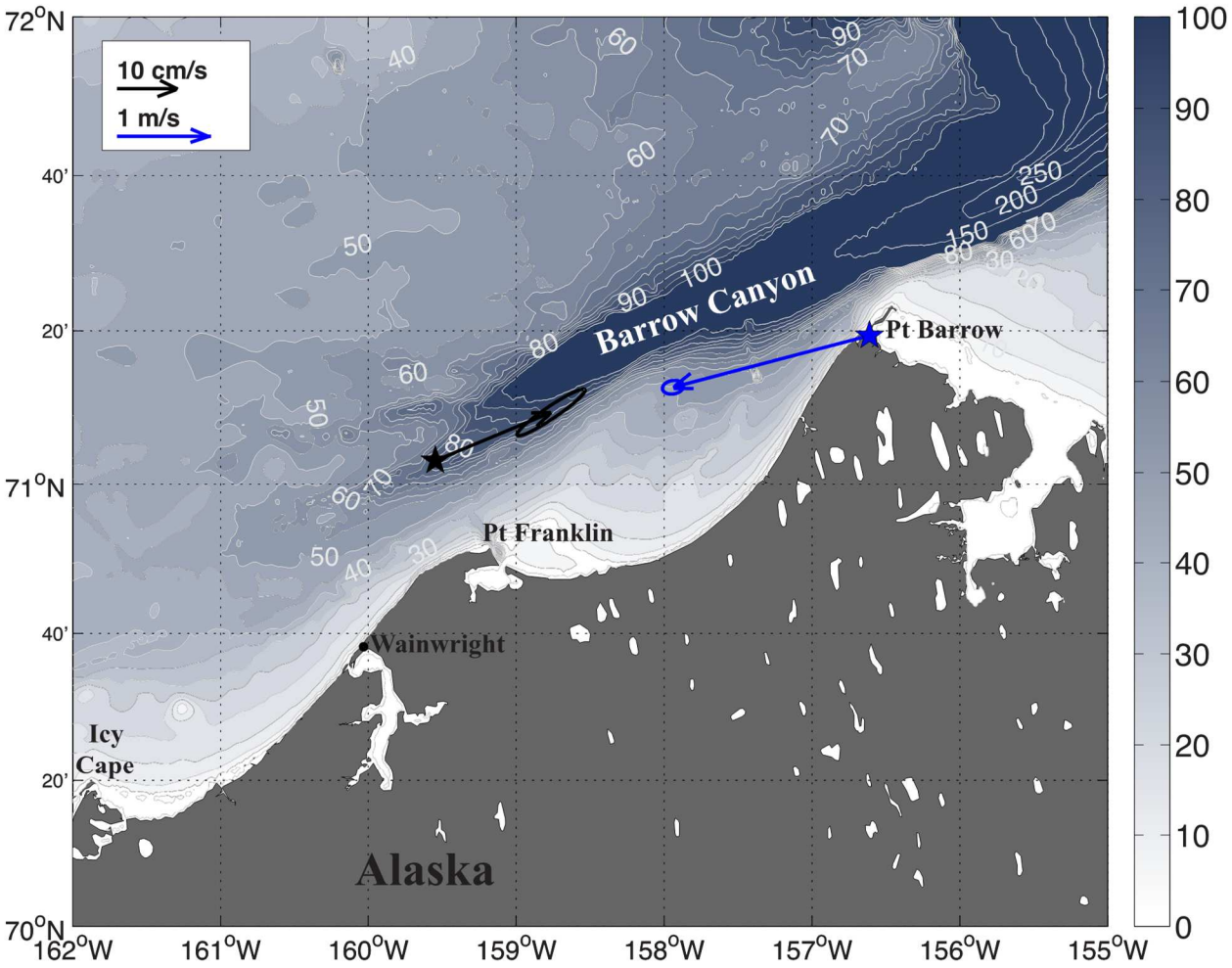

1014

1015 Fig. 2. Enlarged map of the Barrow Canyon region. The location of the SBI mooring used in the study is indicated by
1016 the black star. The location of the Barrow weather station is indicated by the blue star. The mean current and wind
1017 vectors and their standard error ellipses are shown in black and blue, respectively. The bathymetry is the IBCAO v3
1018 product; white numbers indicate depth in meters (Jakobsson et al., 2012).

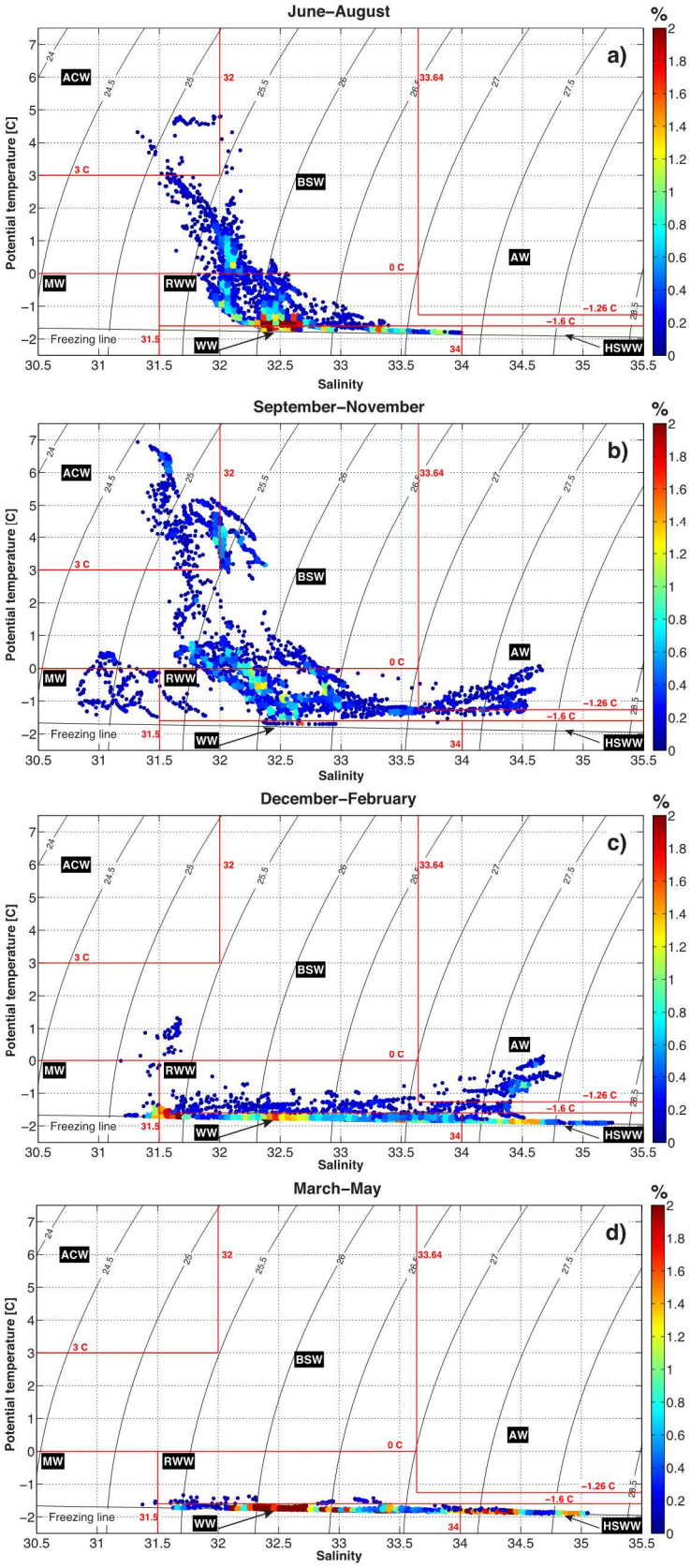

Fig. 3. Seasonal T/S diagrams for the water measured by the mooring, where the color represents the percentage of occurrence of the measurements within bins of 0.05ºC in potential temperature by 0.2 in salinity. (a) June – August; (b) September – November; (c) December – February; and (d) March – May. The water mass boundaries are denoted by the red lines. ACW = Alaskan Coastal Water; BSW = Bering Summer Water; WW = newly ventilated Pacific Winter Water; RWW = remnant Pacific Winter Water; HSWW = hypersaline Pacific Winter Water; MW = Arctic-origin meltwater/river discharge water; and AW = Atlantic Water.

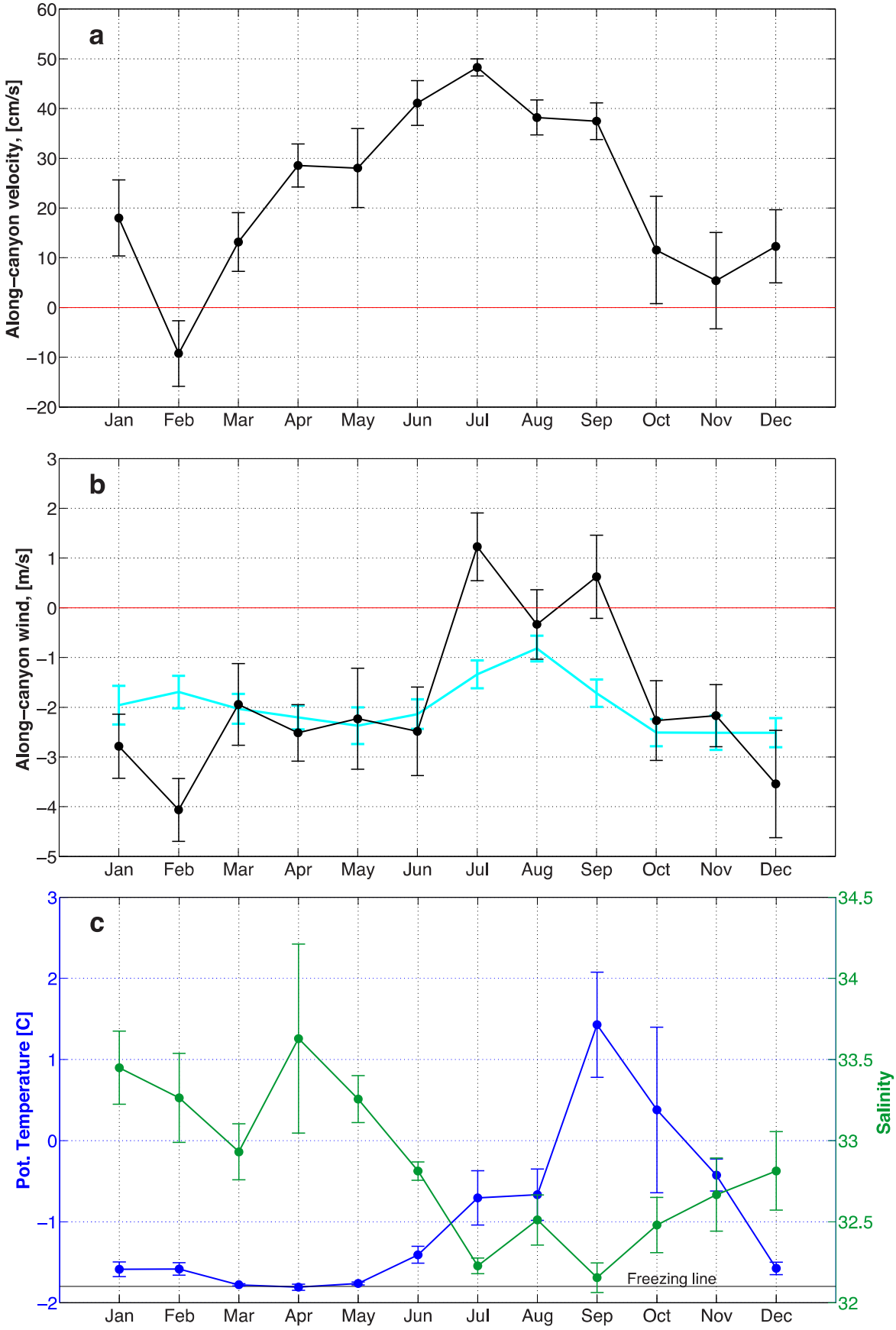

Fig. 4. (a) Monthly means and standard errors for the along-canyon component of the velocity from the mooring near the head of Barrow Canyon deployed from 2002–2004. (b) Same as (a) for the along-canyon component of the wind at Barrow for the mooring deployment period (black curve) and for the climatological period 1979–2014 (cyan), with the standard errors indicated by the bars. Positive values are down-canyon flow/wind. (c) Same as (a) for the potential temperature (blue) and salinity (green) from the mooring. The freezing line is shown in black.

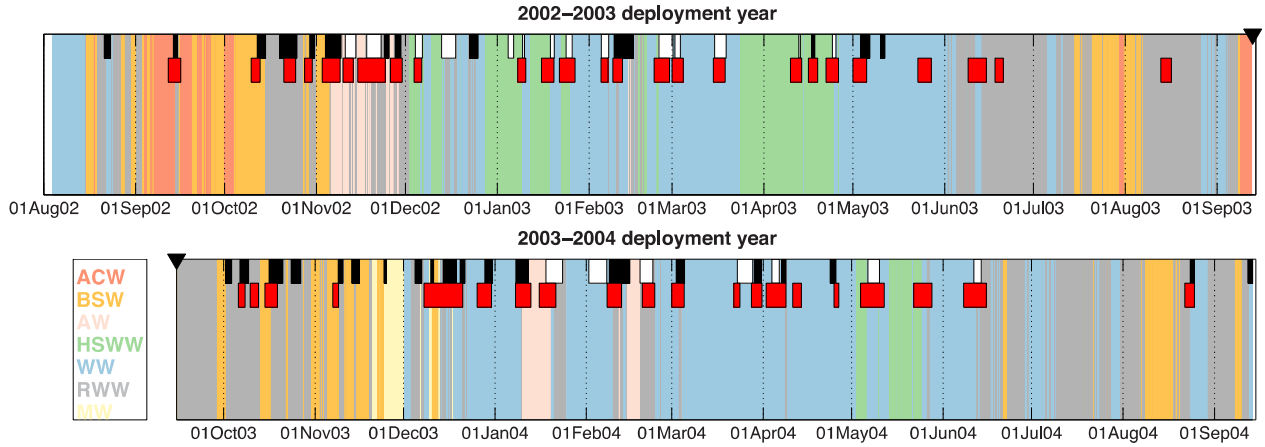

Fig. 5. Time series of water masses using the temperature and salinity data from the mooring at the head of Barrow Canyon. The top panel is the 2002–2003 deployment, and the bottom panel is the 2003–2004 deployment. The mooring turnaround date is denoted by the black triangle in each panel. The different water masses are indicated by the different colors (see the legend). The water mass abbreviations are defined in the caption of Fig. 3. The upwelling events at the head of Barrow Canyon are indicated by the black (positive density anomaly events) and white (negative density anomaly events) patches at the top of each panel. The upwelling events at the Beaufort Slope (Schulze and Pickart, 2012) are indicated by red patches (positive density anomaly events).

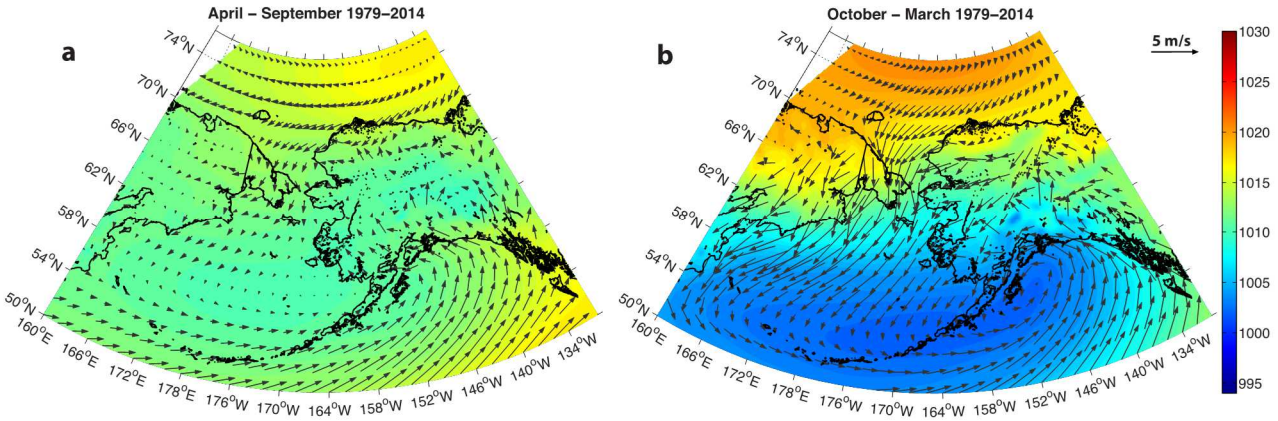

Fig. 6. Maps of climatological mean sea level pressure (mb, color) and 10-m winds (vectors) from NARR for the period 1979–2014. (a) the warm season (April–September); (b) the cold season (October–March).

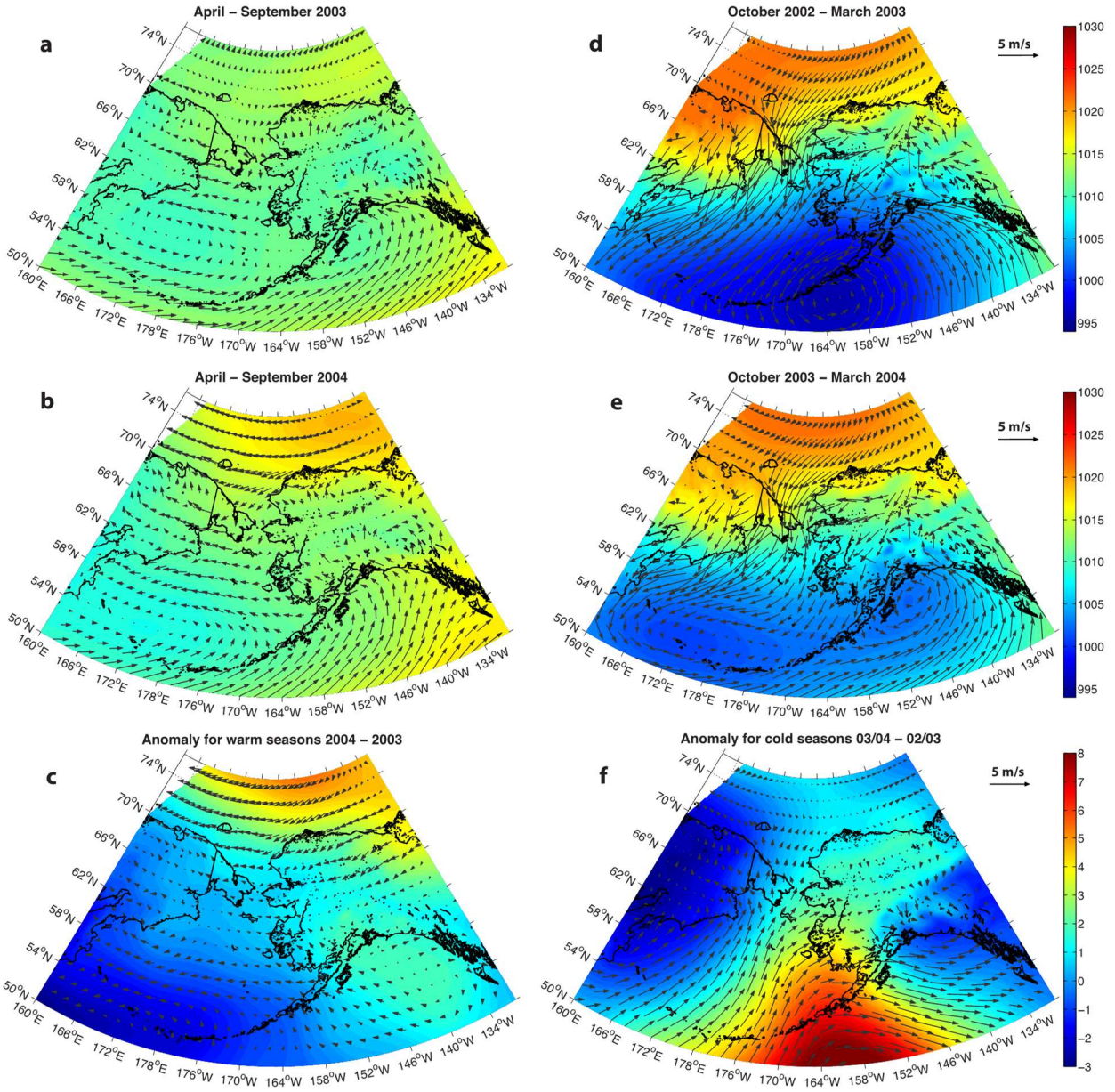

Fig. 7. Maps of sea level pressure (mb, color) and 10-m winds (vectors) from NARR for the warm and cold season of each mooring deployment year, along with the anomaly fields. Left panel (a, b, c): the warm season (April–September); right panel (d, e, f): the cold season (October–March).

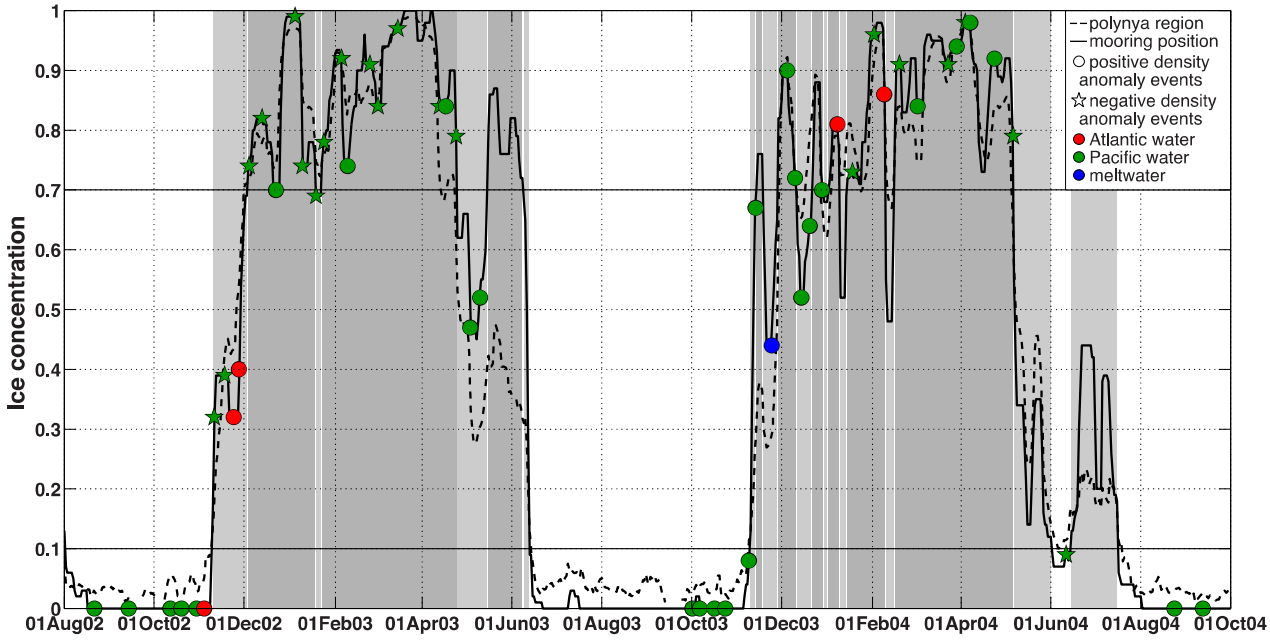

Fig. 8. Ice concentration at the mooring site (solid black line) and median ice concentration within the polynya box (dashed black line) during the two-year mooring deployment (see Fig. 1 for the location of the polynya box). The circles (stars) mark the positive (negative) density anomaly events. The color of the symbols (red, green, blue) mark the water type present at the peak of each event (Atlantic Water, Pacific Water, meltwater respectively). The shading indicates the three ice seasons: open water (white), partial ice cover (light grey), and full ice cover (dark grey).

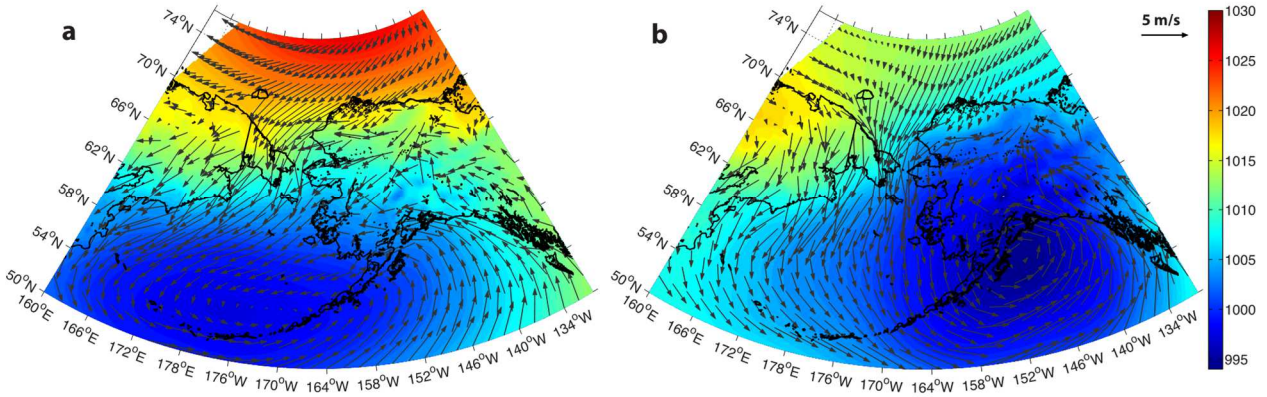

Fig. 9. Composite average maps of sea level pressure (mb, color) and 10-m winds (vectors) from NARR for (a) periods when upwelling occurred along the Beaufort slope as well as at the head of Barrow canyon, and (b) periods when upwelling occurred only in the canyon.

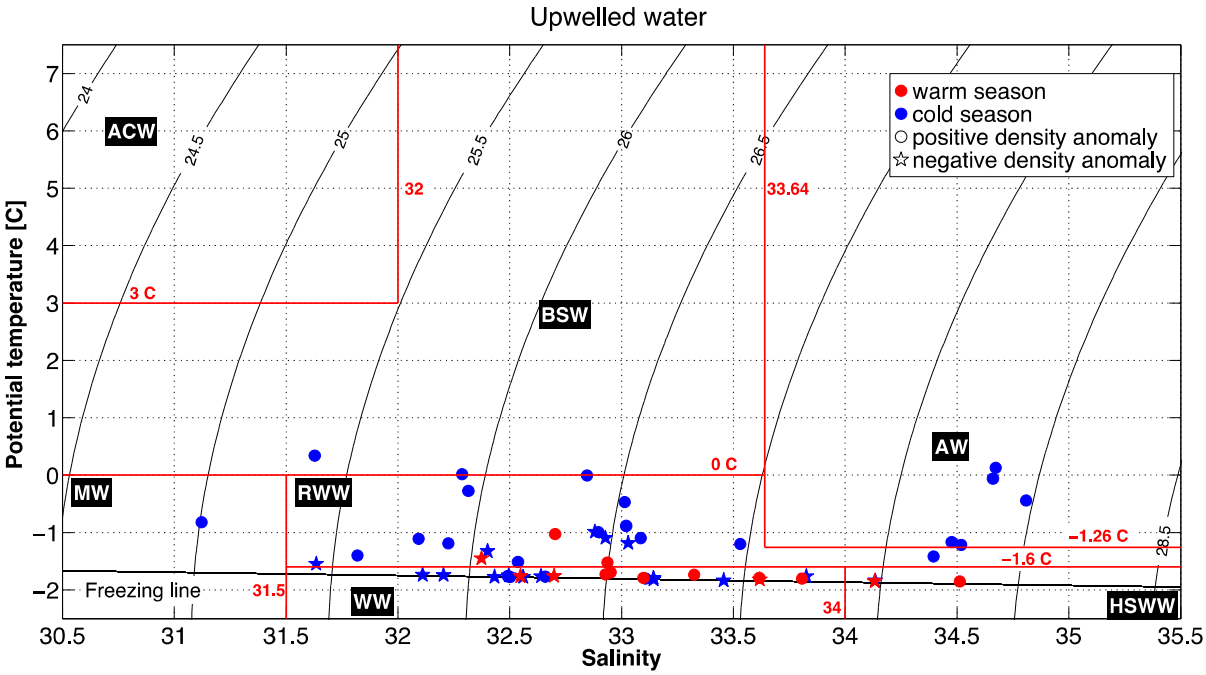

Fig. 10. The T/S value of the water measured by the mooring at the peak of each upwelling event. Red symbols are the events during the warm season, and blue symbols are the events during the cold season. Circles (stars) denote events associated with positive (negative) density anomaly. The water mass definitions are the same as in Fig. 3.

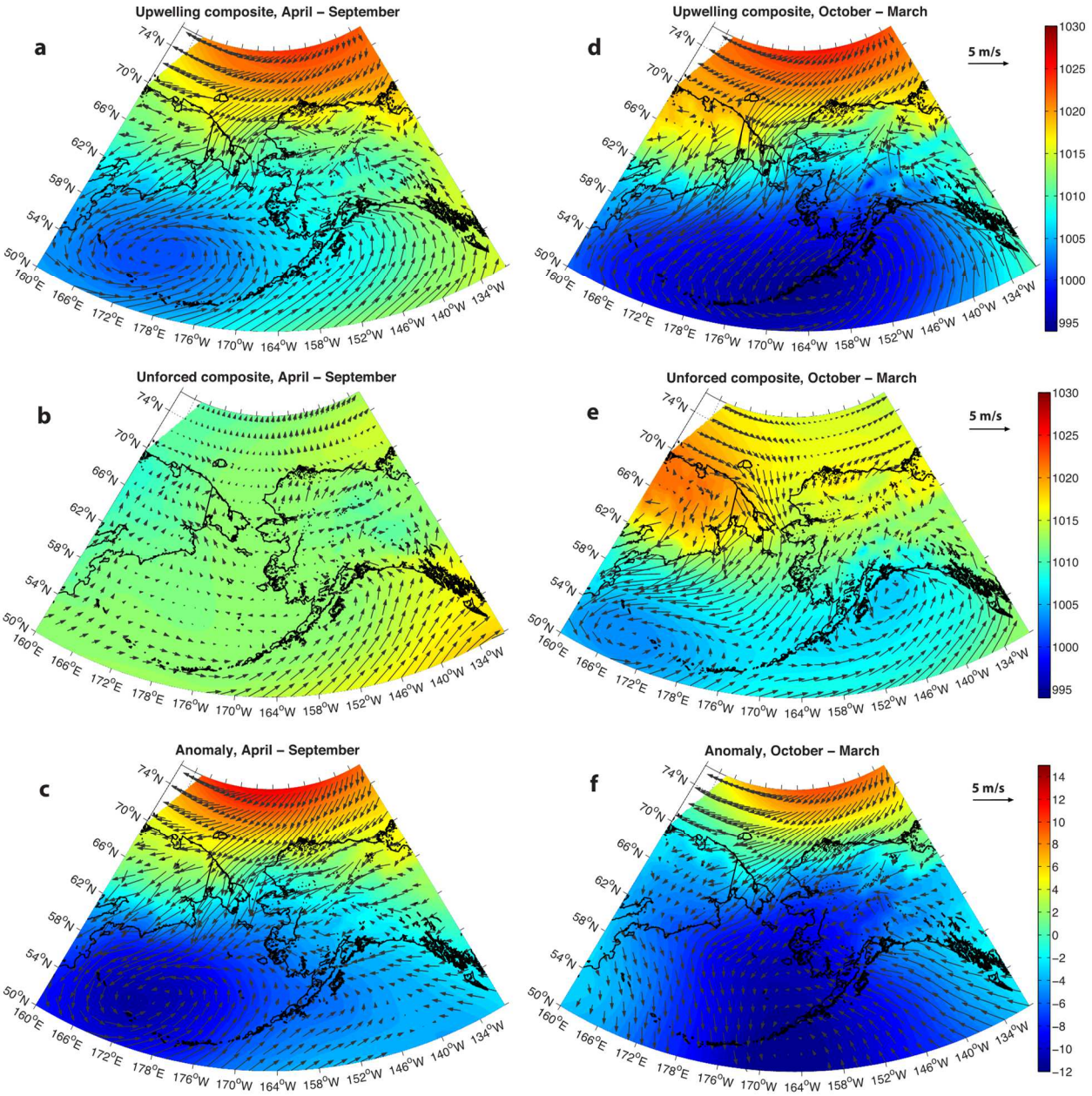

Fig. 11. Maps of sea level pressure (mb, color) and 10-m winds (vectors) from NARR for periods of upwelling (a and d) versus non-forced periods (b and e), along with the anomalies (upwelling minus non-forced, c and f). Left panel (a, b, c): the warm season (April–September); right panel (d, e, f): the cold season (October–March).

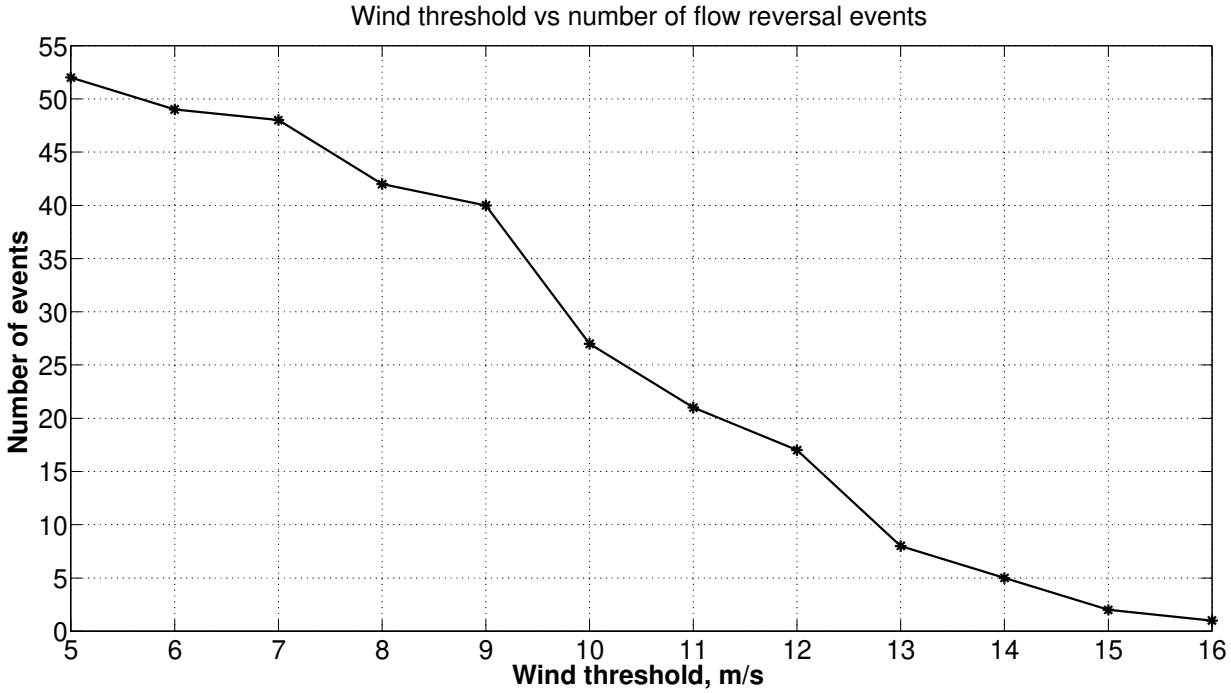

Figure 12. Number of upwelling events as a function of up-canyon wind speed threshold.

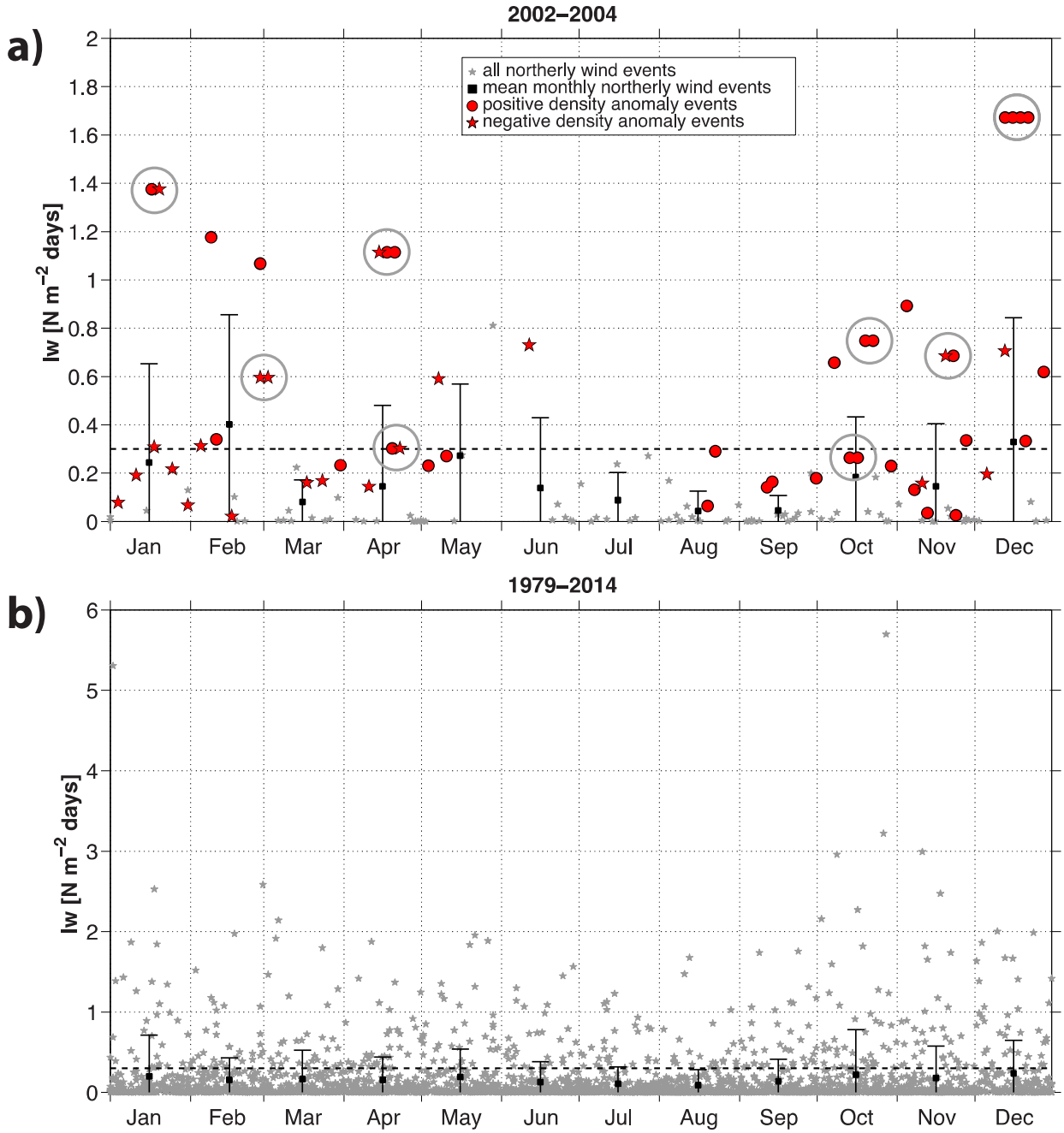

Fig. 13. Time integral of the wind stress I_w for the up-canyon wind events for (a) the mooring deployment period 2002–2004, and (b) the climatological period 1979–2014. The grey stars are the individual events and the black squares are the monthly means. The standard deviations are denoted by the bars. In (a), those events associated with upwelling are indicated by the red circles (positive density anomaly events) and the red stars (negative density anomaly events). The open circles denote multiple upwelling events corresponding to a single storm. The threshold of I_w = 0.3 N m^{-2} d is shown by black dashed line. Note: for presentation purposes the absolute value of I_w is plotted (since it is a negative quantity for northeasterly wind events).

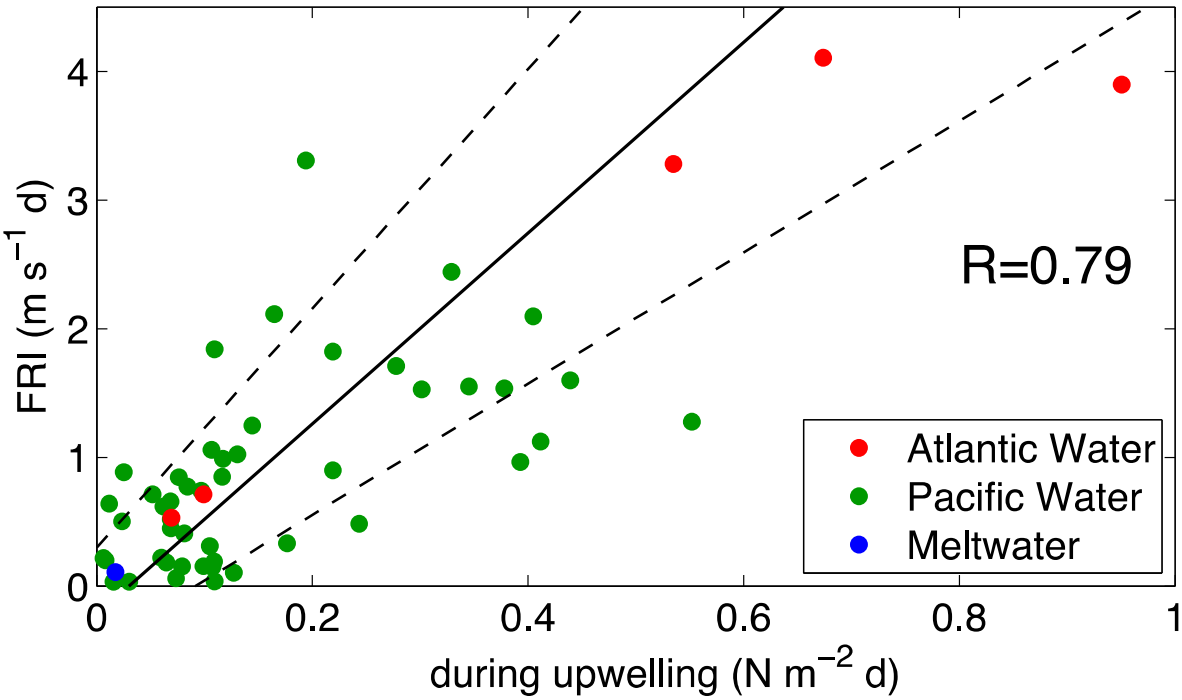

Fig. 14. Value of FRI versus I_w for upwelling events (circles), and the linear fit (black line). The 99% significant levels are indicated by the dashed lines. The color of the symbols (red, green, blue) mark the water type present at the peak of each event (Atlantic Water, Pacific Water, meltwater respectively).

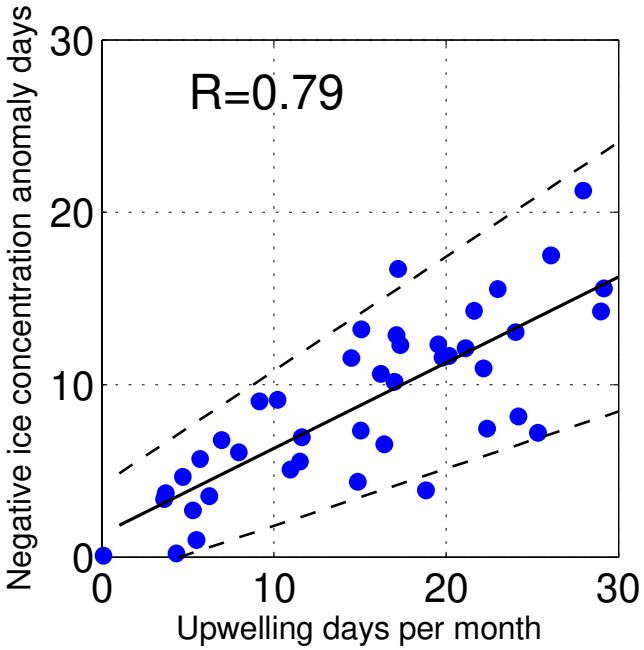

Fig. 15. Number of upwelling days per month versus the number of negative ice concentration anomaly days in the polynya box of Fig. 1 (see text for details). The linear fit is shown (black line) along with the 99% significance levels (dashed lines).